Phosphorus toxicity disrupts Rubisco activation and reactive oxygen species defense systems by phytic acid accumulation in leaves

Daisuke Takagi[1], Atsuko Miyagi[2], Youshi Tazoe[1], Mao Suganami[1], Maki Kawai-Yamada[3], Akihiro Ueda[4], Yuji Suzuki[5], Ko Noguchi[6], Naoki Hirotsu[7], and Amane Makino[1]

[1]Tohoku University
[2]Saitama Daigaku
[3]Saitama University
[4]Hiroshima University
[5]Iwate University
[6]Tokyo Yakka Daigaku Seimei Kagakubu Daigakuin Seimei Kagaku Kenkyuka
[7]Toyo University

May 5, 2020

Abstract

Phosphorus (P) is one of the essential mineral nutrients for plants. Nevertheless, large amounts of accumulated P easily wither whole plants, and this phenomenon is termed as P toxicity. For improving P-use efficiency, to overcome P toxicity is necessary for plant growth. However, the detailed mechanisms underlying P toxicity in plants have not yet been elucidated. In this study, we aimed to investigate the molecular mechanism of P toxicity in rice. We found that, under excessive inorganic-P (Pi) application conditions, Rubisco activation decreased and photosynthesis was inhibited, leading to lipid-peroxidation. Although the defense systems against reactive oxygen species accumulation were activated under excessive Pi application conditions, the Cu/Zn-type superoxide dismutase activity was inhibited. A metabolic analysis revealed that excess Pi application led to an increase in the cytosolic sugar-phosphate content, and activation of phytic acid synthesis. These conditions induced mRNA expressions of the genes that are activated under metal-deficiency conditions, although metals were rather accumulated. These results suggested that P toxicity is triggered by the attenuation of both photosynthesis, and metal availability within cells mediated by phytic acid accumulation. Here, we discuss the whole phenomenon of P toxicity, beginning from the accumulation of Pi within cells to death in plants.

Key words:

Land plants; phosphorus; reactive oxygen species; phytic acid; photosynthesis; plant nutrition

Summary statements: (276 characters including spaces)

Excessive phosphorus application conditions inhibit photosynthesis and attenuate the reactive oxygen species defense systems by stimulating phytic acid synthesis. These physiological responses initiate cell death by oxidative stress, which has observed as phosphorus toxicity.

Acknowledgements:

The authors thank Editage (Cactus Communications Inc.,*https://www.editage.jp/*) for English language editing of the present manuscript. The authors also thank Emer. Prof. Tadahiko Mae, Dr. Hiroyuki Ishida,

and Dr. Keiki Ishiyama of Tohoku University for a fruitful discussion on this manuscript. The authors thank Ms. Louise Thiaville of Tohoku University for her kind language support. The authors thank Prof. Hirohumi Saneoka of Hiroshima University for his technical support.

Conflict of Interest:

The authors declare no conflict of interest.

Author's contributions:

Conceptualization: DT; investigation: DT, AMi, YT, MS, AU, YS, KN, MK, NH; original draft: DT; writing—review and editing: DT, AMi, YT, MS, AU, MK, YS, KN, NH, AMa; funding acquisition: DT, AMa.

INTRODUCTION

In land plants, phosphorus (P) is one of the essential macro-nutrients required to maintain their growth and reproduce seeds for the next generation. P is required in the plant cells as structural constituent of DNA, RNA, phospholipids, and energy coins (ATP, ADP, and AMP) (Hawkesford et al., 2012). In addition, P plays an important role in regulating enzymatic reactions and signaling processes through the protein phosphorylation/dephosphorylation mechanism (Hawkesford et al., 2012). Owing to its role in various physiological functions, the requirement of P in land plants is high followed by the requirements of nitrogen, potassium, calcium, and magnesium among the 17 essential mineral nutrients, and generally, the P content corresponds to approximately 0.2 % of the dry matter of plants (Kirkby, 2012). Land plants can absorb P only in its inorganic phosphate form (Pi) present in the soil through their roots or mycorrhizae (Bieleski, 1973). Land plants possess two kinds of Pi transporters, namely low-affinity and high-affinity transporters (Furihata et al., 1992; Muchhal et al., 1996; Kai et al., 1997; Leggewie et al., 1997; Liu et al., 1998), and their *Km* values are estimated to be 50-100 μM and 2.5-12.3 μM*in planta,* respectively, based on the radioactive Pi uptake experiments (Nussaume et al., 2011). These transporter proteins commonly harbor 12 trans-membrane-spanning regions, with a large hydrophilic charged part dividing the protein molecules into two distinct domains containing of six transmembrane regions in its structure. These transporter proteins transport one Pi with two to four protons (H^+) into the root against the electrochemical and concentration gradients across the root surface (Ullrich-Eberius et al., 1981, 1984; Sakano, 1990; Mimura, 1999; Raghothama, 1999). In this process, the plasma membrane H^+-ATPase contributes to generating the H^+ electrochemical gradient and maintaining the cytoplasmic pH for Pi/H^+ symport (Ullrich-Eberius et al., 1981, 1984; Mimura, 1999; Raghothama, 1999). The Pi acquisition strategy in land plants is sophisticated and well-regulated from the transcriptional- to the post-translational level (Secco et al., 2012; Gu et al., 2016). Under conditions of low Pi availability, the expression of Pi transporter genes is activated by Pi-starvation responsive transcription factors such as PHR protein-harboring MYB-domain and WRKY-proteins (Rubio et al., 2001; Zhou et al., 2008; Gu et al., 2016). In addition, microRNA399 and microRNA827 support Pi uptake and accumulation in plants at the post-transcriptional step (Fujii et al., 2005; Aung et al.,2006; Bari et al., 2006; Chiou et al., 2006; Franco-Zorrilla et al., 2007; Lin et al., 2010; Secco et al., 2012; Gu et al., 2016). Simultaneously, a negative feedback system to suppress the excess Pi uptake is switched on, such as the increase in class 1 SPX domain-containing proteins, which suppress the expression of Pi-starvation responsive genes, and the non-protein cording gene*IPS1,* which acts as a target-mimicry of microRNA399 under Pi starvation conditions (Franso-Zorrilla et al., 2007; Wang et al., 2009; Liu et al., 2010; Secco et al., 2012; Puga et al., 2014; Wang et al., 2014). In contrast, under conditions of adequate Pi availability, the Pi transporters are actively degraded by an E2 ubiquitin conjugase-related protein, PHO2, thus leading to the down-regulation of Pi absorption (Delhaize & Randall, 1995; Dong et al., 1998; Aung et al., 2006; Bari et al., 2006). After Pi absorption from the rhizosphere, the Pi homeostasis functions in plant cells (Biddulph et al., 1958; Lee et al., 1990; Mimura, 1995, 1999). When Pi is sufficiently supplied to the cells, Pi is stored in vacuoles to maintain its concentration in the cytosol and organelles such as chloroplasts and mitochondria (Mimura et al., 1990, 1992, 1996; Pratt et al., 2009). On the other hand, under Pi deficiency, Pi is exported from the vacuoles to the cytosol and is preferentially distributed into various organelles for maintaining cellular physiological

functions (Mimura et al., 1990, 1992, 1996; Pratt et al., 2009).

As mentioned above, although Pi is essential for plant growth, excess Pi application to plants leads to chlorosis and necrosis in the leaves and finally withering in whole plants. These phenomena have been recognized as P toxicity (Rossiter, 1951; Bhatti & Loneragan, 1970; Clarkson & Scattergood, 1982). To our knowledge, P toxicity has been first reported in 1917 by John W. Shive (Shive, 1918). He examined the effect of different levels of P application on soybean growth by the soil and water culture method, concluding that excess Pi application causes specific injury in soybean leaves (Shive, 1918). Such P toxicity symptoms have been observed in the leaves of various land plant such as rice, wheat, barley and *Arabidopsis* (Bhatti & Loneragan, 1970; Aung et al., 2006; Chiou et al., 2006; Wang et al., 2009; Liu et al., 2010). In general, P toxicity occurs when the Pi content exceeds approximately 1% of the dry matter of leaves (Bhatti & Loneragan, 1970). P toxicity has been assumed to be caused by zinc (Zn)-deficiency in the leaves because the Zn content decreases depending on the dosage of Pi application in plants (Singh et al., 1988; Zhu et al., 2001; Zhang et al., 2002; Hawkesford et al., 2012). Several hypothetical mechanisms have been proposed to explain P-induced Zn-deficiency in plants. Some of the major mechanisms include: 1. the dilution effect of Zn on the tissue growth stimulated by P application; 2. inhibition of Zn absorption by root under excess P application through mineral interaction in soil (Loneragan et al., 1979); 3. suppression of Zn translocation from root to shoot (Singh et al., 1988); 4. inhibition of Zn acquisition depending on mycorrhizae under excess P application (Ova et al., 2015). In contrast, several studies have shown that P toxicity is observed in plant leaves despite normal Zn accumulation in the leaves (Loneragan et al., 1979; Cakmak & Marschner, 1987; Ova et al., 2015). Therefore, P toxicity cannot be explained only by the suppression of Zn acquisition from soil to leaves. Interestingly, Delhaize and Randall (1995) observed that light intensity directly modulates the P toxicity symptoms in a Pi-accumulating *Arabidopsis* mutant (*pho2*), and limiting the illumination alleviates P toxicity. This observation implies the involvement of photosynthesis in the occurrence of P toxicity, but the detailed molecular mechanisms of P toxicity have not yet been addressed in land plants.

In this study, we investigated the detailed mechanisms of P toxicity that cause withering in land plants, especially in the leaves. Firstly, we examined the effects of Pi application on photosynthesis, and subsequently, found that high Pi application simultaneously limits photosynthesis and decreases in the scavenging activity of reactive oxygen species (ROS), as a result of the lower availability of metals caused by phytic acid synthesis in leaves. Thereafter we discussed the detailed whole phenomenon of P toxicity in land plants.

MATERIALS AND METHODS

Plant growth conditions

Oryza sativa L. 'Notohikari' wild-type, Rubisco-sense and antisense rice plants were used (Makino et al., 2000; Suzuki et al., 2007). Seeds were imbibed at 30 °C for three days and were subsequently grown on a plastic net floating on tap water for 3 weeks in an environmentally controlled phytotron (NK system, Japan). Subsequently, rice seedlings were grown in hydroponic culture (Makino et al., 1994). Here, we used six different Pi application conditions by changing NaH_2PO_4 concentration: 0.06 (low-Pi), 0.6 (control-Pi), 1.2,1.8, 2.4, and 3.0 mM. Na^+concentration was normalized by applying NaCl. The pH of the hydroponic culture was adjusted to 5.2 with 6 M HCl, and it was replenished twice in a week. The chamber was maintained at 60 % relative humidity with a 14-h light (28 °C) and a 10-h dark (25°C) photoperiod. The light intensity was 500-600 μE m^{-2} s^{-1}. All physiological and genetical analyses were performed for fully and newly expanded leaves after 70 days of their germination.

Chlorophyll (Chl) and nitrogen (N) content measurements

Leaf Chl content and Chl *a* /*b* ratio were determined as reported previously (Takagi et al., 2019). In brief, leaf segments were incubated in *N, N* -dimethylformamide at 4 °C overnight and the absorbance values of the aliquot were measured at 750 nm, 663.8 nm, and 646.8 nm to calculate the chlorophyll content (Porra et al., 1989). The total leaf nitrogen content was determined by using the Nessler's reagent in a digestion solution after the addition of potassium sodium tartrate ($KNaC_4H_4O_6$) and then measuring the absorbance at 420 nm (Takagi et al., 2017).

Inorganic phosphate (Pi) and organic phosphate (Po) quantifications

Leaf Pi and Po contents were quantified by the molybdenum blue method according to Kurita et al. (2014).

Measurements of photosynthetic activities

Gas exchange analysis, Chl fluorescence and $P700^+$ were simultaneously measured using a combined system of GFS-3010 and Dual-PAM-100 (Heinz WalzGmbH, Germany). Ambient air (40 Pa CO_2, 21 kPa O_2) and gases with pure CO_2 were mixed to determine the CO_2concentration during measurements. The gases were saturated with water vapor at 18.0±0.1 °C, and the leaf temperature was maintained at 25 °C. The following Chl fluorescence parameters were calculated as described by Baker (2008): Fo, minimum fluorescence yield; Fm, maximum fluorescence yield; Fm', maximum fluorescence yield under the illumination; and Fs, steady-state fluorescence yield. A measuring light (0.1 μE m^{-2} s^{-1}) and a saturated pulse (20,000 μE m^{-2} s^{-1}, 600 ms) were applied to determine Fo, Fm, and Fm'. The oxidation-reduction state of P700 in photosystem (PS) I was determined according to the method of Klughammer & Schreiber (1994). The maximum oxidation level of P700 (Pm) was obtained using a saturated pulse under far-red light illumination. The oxidation–reduction state of P700 was determined using the oxidation level of P700 at the steady-state (P) and the maximum oxidation level of P700 under illumination (Pm'). For determining the*proton motive force* (*pmf*), H^+-efflux conductance (gH^+), and H^+-efflux rate (V_{H^+}) in leaves, the electrochromic shift (ECS) was measured using the dark interval relaxation kinetics-analysis (Sacksteder & Kramer, 2000). The value of*pmf* was normalized by the ECS-signal obtained by a single-turnover flash (10 μs) (Takagi et al., 2017). Actinic red light (AL) was used to measure the photosynthetic parameters.

Inductively coupled plasma atomic emission spectroscopy (ICP-AES) measurement

Leaf mineral content was determined according to Mekawy et al. (2018). A leaf blade was dried at 80 °C for 1 day and was crushed by μT-48 (TAITEC, Japan). The crushed samples were decomposed in an acid mixture (HNO_3:H_2SO_4:$HClO_4$= 5:1:2) overnight. Subsequently, the solution was heated at 150°C for 30 min in a heat block. After cooling, the solutions were heated again at 200 °C for 1 h. The above process was continued until the solutions became colorless. The obtained solutions was were for ICP-AES analysis (iCAP6000; Thermo-Fisher, Japan).

Sodium dodecyl sulfate-polyacrylamide gel electrophoresis (SDS-PAGE) and Western blot analysis

SDS-PAGE and Western blotting were performed as previously described (Takagi et al., 2017). In belief, the extracted proteins were electrophoresed on 12.5% (w/v) polyacrylamide gels containing 0.1% (w/v) SDS and 6 M urea. Proteins were separated using SDS-PAGE, transferred onto polyvinylidene difluoride (PVDF) membranes and then blocked with skimmed milk for 30 min at 25 °C. The PVDF membranes were subsequently incubated with a polyclonal antibody specific for Rubisco activase (Agrisera, Sweden) for 1 h at 25 °C. The target proteins were detected by SuperSignal West Dura Extended Duration Substrate kit (Thermo Fisher Scientific K.K., Japan) and LAS-4000 (Fuji film, Japan). The target protein content was determined by using the Image J software (National Institutes of Health, USA).

Metabolite analysis

Sugar-phosphates were extracted as previously described by Noguchi et al. (2018). Leaves were sampled under illumination at 1,100 μE m^{-2} s^{-1} in ambient air (40 Pa CO_2, 21kPa O_2, 25 °C), and immediately frozen in liquid N_2. The frozen leaves were ground with a mortar and pestle in liquid N_2. Methanol was added to the homogenized leaves, and same volume of a solution containing internal standards (100 μM PIPES and 100 μM methionine sulfone) were mixed after vortex. After centrifugation, the resulting supernatants were filtered through a 3 kDa cut-off filter (Millipore) at 16,100×g at 4°C for 30 min. The sugar-phosphates were separated by capillary electrophoresis-triple quadrupole-mass spectrometry (CE-QQQ-MS; 7100 Capillary Electrophoresis, MS; 6420 Triple Quad LC/MS, Agilent Technologies, USA) with multi reaction monitoring mode as described previously (Miyagi et al. 2010, 2019). All CE-QQQ-MS data were processed using the Agilent MassHunter software (Agilent Technologies).

Rubisco assay

The Rubisco content in a leaf bade was determined as described by Makino et al. (1986). Rubisco was separated by SDS-PAGE and stained with Commassie Brilliant Blue R-250 (CBB-R). Subsequently, the Rubisco protein bound to CBB-R was cut out from the SDS-PAGE gel and extracted with formamide at 50 °C for 5 h. The absorption of the extract was measured at 595 nm, and the Rubisco content was determined.

Rubisco activation was determined as described by Suganami et al. (2018). A leaf blade was illuminated at an irradiance of 1,100 μE m^{-2} s^{-1} and 25 °C under ambient air conditions (40 Pa CO_2, 21 kPa O_2) for at least 1 h, and the illuminated leaf was immediately frozen in liquid N_2. The frozen leaf was homogenized in the Rubisco extraction buffer [100 mM 4-(2-hydroxyethyl)-1-piperazineethanesulfonic acid (HEPES) / NaOH (pH 8.0), 20 mM $MgCl_2$, and 10 mM dithiothreitol (DTT)] with quartz sand on ice and centrifuged (19,000×g , 10 s at 4°C) to obtain a solution containing Rubisco. Rubisco activation was determined by multiplying the initial activity with the maximum activity, and the carbamylation potential was determined by multiplying the total activity with the maximum activity.

Measurement of ascorbate peroxidase (APX) and superoxide dismutase (SOD) activities

A leaf blade was homogenized by the enzyme extract solution [50 mM potassium phosphate buffer (pH 7.0), 1 mM EDTA, 20% (w/v) sorbitol, 5% (w/v) polyvinylpyrrolidone, 1% (w/v) Tween-20, and 1 mM ascorbate] with quartz sand. The APX activities were measured by following Amako et al. (1994). The SOD activities were measured according to Flóhe & Ötting (1984).

Real-time PCR analysis for mRNA quantification

mRNA was purified from rice leaf blade as described by Suzuki et al. (2004). The total RNA was quantified by measuring the absorbance at 260 nm. The real-time PCR analysis was conducted using the StepOnePlus Real-Time PCR System (Applied Biosystems, USA) and Fast SYBR Green Master Mix (Life technologies Japan) (Ogawa et al., 2012). The primers used for mRNA expression analysis are listed in Table S1.

Lipid hydroperoxide quantification

Lipid hydroperoxide (LOOH) in rice leaf blade was quantified by using Spy-LHP (Dojindo, Japan) (Chan et al., 2012). A leaf blade was homogenized in the extraction buffer [Pottasium-phosphate buffer (pH 7.0). 1 mM EDTA, 12.5% (v/v) Glycerol], and the resulting leaf extract was incubated with 2.7 μM Spy-LHP for 30 min on ice. After centrifugation, the supernatant was monitored for fluorescence emission (RF-1500, Shimazu). The excitation and emission wave lengths were 520 and 540 nm, respectively.

Phytic acid quantification

Phytic acid content was measured in accordance with Perera et al. (2019). Fully expanded leaves were homogenized in 0.66 M HCl with quartz sand, and phytic acid was extracted by shaking the homogenized solution at 25 °C for 17 h. The extracts were centrifuged (19,000×g , 10 min at 4 °C) and the supernatant was neutralized with 0.75 M NaOH. The phytic acid content was measured by using the Phytic Acid (Total Phosphorus) Assay Kit (Megazyme International Ireland Ltd., Ireland).

Statistical analysis

All measurement data were expressed as mean ± SD of at least three independent biological analyses. For the detection of differences among the rice plants grown under different Pi conditions or rice mutants, we used the one-way analysis of variance (ANOVA) and Tukey-Kramer's honest significant difference (HSD) test. All statistical analyses were performed using the software program Origin Pro 2019 (LightStone Corp., Japan).

RESULTS

Effects of Pi application and P toxicity on rice plants

To investigate the effects of the Pi application, wild-type rice plants (WT) were grown under six different Pi levels ranging from 0.06 to 3.0 mM (Figure 1). Compared to the low-Pi and control-Pi treatments (0.06 and 0.6 mM), higher Pi application (above 1.2 mM) caused chlorosis and necrosis at the tip of the leaf blade (Figure 1a). Such a phenomenon has been observed previously in rice plants that accumulate excess Pi (Aung et al., 2006; Wang et al., 2009; Liu et al., 2010). The plant height was not affected by Pi application (Figure 1b). The Chl content of the leaf blade was the highest in the plants treated with 0.06 mM Pi and decreased gradually with increasing Pi application (Figure 1c). The total dry weight including roots was reduced in the 0.06 mM Pi treatments, and Pi applications higher than 1.2 mM further decreased the dry weight (Figure 1d). The leaf sheath weight was the most susceptible to an increase in Pi application, and Pi levels higher than 1.8 mM significantly decreased the leaf sheath weight compared to the control-Pi treatments (Figure 1d).

To confirm whether different Pi application levels affect the P content in leaves, the Pi and organic phosphate (Po) content in the leaf blade were determined per unit of fresh weight (F.W.) and leaf area. The Pi content increased with increasing Pi application, and Po content also increased, but to a lesser extent (Table 1). These results indicated that Pi is accumulated in leaves, depending on the Pi concentration, and P toxicity can be caused in WT rice plants growing under Pi conditions higher than the control-Pi conditions.

Excessive Pi application declines the Rubisco-limited photosynthesis

Because the onset of P toxicity symptoms requires illumination, the photosynthetic metabolism should provide an insight into the cause of P toxicity under illumination conditions. We measured the CO_2 assimilation rate (A), and quantum yield of photosystem (PS) II [Y(II)], for dissipation by down-regulation [Y(NPQ)], and for other non-photochemical losses [Y(NO)] (Kramer et al., 2004) as a function of the internal partial pressures of CO_2 in the leaves (Ci) of rice plants grown under different Pi conditions. The low-Pi plants showed lower A than the control-Pi plants, especially at high Ci levels (Figure 2a). The Y(II) was lower in the low-Pi plants than in the control-Pi plants at high Ci levels (Figure 2b). In contrast, the low-Pi plants showed higher Y(NPQ) than the control-Pi plants at high Ci levels (Figure 2c). However, the low-Pi and control-Pi plants showed similar Y(NO) (Figure 2d). These responses showed a typical Pi limitation in photosynthesis (Sharkey, 1985; Fabre et al., 2019), and lowering Pi decreased $A$by limiting the Pi turnover, and NPQ was stimulated to protect the photosynthetic electron transport (PET) system at high Ci levels.

On the other hand, A decreased with an increase in Pi application above 1.2 mM Pi (Figure 2e). In addition, the response to Ci became more linear. The initial slope of A: Ci was the highest in the control-Pi plants and decreased with increasing Pi application (Figure 2i). Because the initial slope of A :Ci suggested Rubisco activity (von Caemmerer & Farquhar, 1981), these results indicated that the Rubisco activity decreased with increasing in Pi application. An increase in Pi application lowered Y(II) in the wide range of Ci, and the response of Y(II) to Ci also became linear in a manner similar to that of A (Figure 2f). Y(NPQ) increased with an increase in Pi application, but was suppressed at low Ci levels in the 3.0 mM Pi plants compared to the control-Pi plants (Figure 2g). Y(NO) was similar in all the Pi applications except for the 3.0 mM Pi conditions (Figure 2h). This implied that although NPQ is stimulated with increasing Pi accumulation in the leaves, excessive Pi accumulation disturbs the redox-state of the PET chain. In fact, the Fv/Fm value was significantly decreased in the 3.0 mM Pi treatments (Figure 2j).

For detailed effects of excessive Pi application on photosynthesis, we also examined the PSI parameters [Y(I), Y(ND), and Y(NA)] and H^+-management within the chloroplasts [*proton motive force* (*pmf*), H^+-conductance in chloroplastic ATPase (gH^+) and H^+-efflux rate in chloroplastic ATPase (V_{H^+})] in the plants grown under low-Pi, control-Pi, and 3.0 mM Pi conditions. Y(I) indicates the photochemical quenching in PSI, whereas Y(ND) and Y(NA) indicate the photosynthetic electron transport limitation at the donor and acceptor sides of PSI, respectively (Klughammer & Schreiber, 1994). Y(I) showed a response similar to Y(II) (Figure S1a). Y(ND) decreased with increasing Ci levels both under low-Pi and control-Pi conditions (Figure S1b). Y(ND) in the 3.0 mM Pi plants decreased with an increase in Ci, but the values were higher than those in the low-Pi and control-Pi plants (Figure S1b). Y(NA) increased with increasing Ci in both low-Pi and control-Pi plants, but Y(NA) was higher in the low-Pi plants than in the control-Pi plants (Figure S1c).

In contrast, the 3.0 mM Pi plants showed the highest Y(NA) at low Ci levels, and Y(NA) was maintained at higher levels in the 3.0 mM-Pi plants than in the control-Pi plants (Figure S1c). These results indicated that the low-Pi plants reduced PSI at higher Ci with photosynthesis limitation, but the 3.0 mM Pi plants caused a disturbance in the redox-state of PSI, shifting PSI to a more reduced state, despite the donor-side PET limitation in PSI.

The*pmf* and $g_H{}^+$ were similar between the control-Pi and low-Pi plants, but $V_H{}^+$ was slightly lower in the low-Pi plants than in the control-Pi plants (Figure S2). In contrast, the 3.0 mM Pi plants showed lower *pmf* , $g_H{}^+$, and $V_H{}^+$ than the control-Pi plants (Figure S2). Both $g_H{}^+$ and $V_H{}^+$ showed linear responses to Ci in a manner similar to A , Y(II), and Y(I) (Figure 2e, f and Figure S1a). These results indicated that both *pmf* generation by PET reaction and ATP synthesis are suppressed under 3.0 mM Pi conditions (Takagi et al., 2016b, 2017). These observations indicated that excessive Pi accumulation suppressed photosynthesis over a wide range of Ci levels, and this phenomenon was different from that caused by low Pi application in rice plants.

Excessive Pi application increases sugar-phosphate content in both chloroplasts and cytosol

To evaluate the effects of excessive Pi application on sugar-phosphate metabolism, we analyzed the content of major sugar-phosphates and adenylates in leaves under

illumination conditions (see Materials and Methods). In the low-Pi plants, a large number of sugar-phosphates were decreased compared to the control-Pi plants (Figure 3b). However, ribose-5-phosphate (R5P) showed similar levels in both low-Pi and control-Pi plants, and the levels of ribulose-5-phosphate (Ru5P) and glycerol-3-phosphate (G-3-P) were higher in the low-Pi plants than in the control-Pi plants. The total adenylate content was lower in the low-Pi plants than in the control-Pi plants, and the ATP/ADP ratio was also decreased (Figure 3c, d). These results indicated that the substrates for photosynthesis in the Calvin cycle decreased, and that the ATP consumption exceeded the ATP synthesis owing to lower adenylate content in low-Pi plants than in the control-Pi plants. These observations were clearly consistent with the photosynthetic kinetics in the low-Pi plants (Figure 2a) (Sharkey, 1985; Fabre et al., 2019). The increases in Ru5P and R5P levels in the low-Pi plants might be caused by limited ATP supply (Figure 3a, b). The increase in G-3-P has been observed under P deficiency for remodeling lipid composition (Cheng et al., 2011; Nakamura, 2013), that is, an increase in G-3-P represents the P starvation response (Figure 3b). An increase in Pi application increased the sugar-phosphate content (Figure 3b). Especially, the levels of glycelaldehyde-3-phosphate (GA3P), dihydroxyacetone-phosphate (DHAP), fructose-6-phosphate (F-6-P), 6-phospho gluconate (6-PG), glucose-1-phosphate (G-1-P), and glucose-6-phosphate (G-6-P) were increased with an increase in Pi application (Figure 3b). The total adenylate levels were also increased with an increase in Pi application (Figure 3c). In contrast, the ATP/ADP ratio was enhanced with increasing Pi application (Figure 3d). These results indicated that the ATP consumption is suppressed more than the ATP synthesis under high Pi application conditions. This observation clearly matched the decrease in the H^+-conductance of the chloroplastic ATP synthase as indicated by the value of gH^+ (Figure S2b).

Excessive Pi application does not affect the content of Rubisco content, but declines Rubisco activation

The total leaf N content significantly decreased in the low-Pi treatments and remained almost constant above 1.2 mM Pi treatments (Figure 4a). The Rubisco content showed a similar response to the total leaf N content. A low-Pi application slightly decreased the Rubisco content, but a higher Pi application did not change the Rubisco content (Figure 4b).

Rubisco activation maintained high in the low-Pi treatments, but decreased with increasing Pi application (Figure 4c). The carbamylation potential of Rubisco, which is lowered by a tight binging inhibitor, such as 2-carboxy-D-arabinitol 1-phosphate, was not different among different levels of Pi application (Figure 4d). Indeed, the Rubisco in the night-sampled leaves showed significantly lower activation and carbamylation potential compared with the Rubisco sampled under illumination (Figure 4c, d). Thus, one of the reasons for the decline in photosynthesis by excessive Pi application is a decline in *in vivo* Rubisco activation.

Because Rubisco activation is catalyzed by Rubisco activase (RCA) (Salvucci et al., 1985), we examined the RCA content of the leaves. Three different isoforms of RCA resulting from alternative splicing and limited proteolysis have been reported in rice plants (Portis 2003; Vargas-Suarez et al., 2004; Fukayama et al., 2012). According to Fukayama et al. (2012), an upper protein band corresponds to theα- form of RCA, which has redox-active cysteine residues; a middle protein band corresponds to the β -form, which lacks redox active Cys residues; and a lower protein band corresponds to the N-terminal processed β (β^*)-form in the leaves (Figure 4e). The total amount of RCA, including the α- , β-, and β^*- forms was similar among different Pi treatments (Figure 4f). However, a high-Pi application decreased the content of α - andβ -forms compared with the control-Pi conditions (Figure 4g). Contrary to the change in the α- and β -forms, theβ^* -form content increased with increasing Pi application (Figure 4g). When the isoform ratios of α /β and β */βwere calculated, an increase in Pi application decreased theα /β ratio and increased the β */β ratio, compared to the low-Pi and control plants (Figure 4h, i). These results indicated that an increase in Pi application modified the RCA isoform composition of the leaves.

Excessive Pi application stimulates the ascorbate peroxidase (APX) activity but suppresses the Cu/Zn-superoxide dismutase (SOD) activity

As shown in Figure 2 and Supplemental Figures S1 and S2, an increase in Pi application limited photosynthesis and reduced the PET chain in the leaves. These results implied that ROS production is stimulated under P toxicity conditions (Cakmak, 2005; Takagi et al., 2016a). Based on this consideration, the ascorbate peroxidase (APX) and superoxide dismutase (SOD) activities were measured as key candidates for ROS-scavenging enzymes. The total APX activities, including the cytosolic and chloroplastic APX activities, tended to be higher in the 2.4 and 3.0 mM Pi treatments than in the other Pi treatments (Figure 5a). The cytosolic APX activity did not differ among the Pi treatments, but the chloroplastic APX activity was significantly increased in the 3.0 mM Pi treatments (Figure 5a). The increase in chloroplastic APX activity in the 3.0 mM Pi treatments was also observed on the leaf Chl content basis (Figure 5b). In contrast, a higher Pi application significantly decreased the total SOD activities, including the Fe-, Mn-, and Cu/Zn-SOD activities (Figure 5c). A decrease in the total SOD activities under excessive Pi application was also reported by Cakmak and Marschner (1987). The decrease in total SOD activities was due to the significant decrease in the Cu/Zn-SOD activity rather than a decrease in the Fe-, Mn-SOD activities (Figure 5c).

To understand the general response of APX and SOD activities under the limitation of photosynthesis, the APX and SOD activities were measured in the Rubisco-sense and antisense plants (Figure S3a) (Makino et al., 2000; Suzuki et al., 2007). Under the control-Pi conditions, the Rubisco-antisense plants showed significantly higher total and chloroplastic APX activities than the WT and Rubisco-sense plants, although the cytosolic APX activity was similar among them (Figure S3b, c). Under 3.0 mM Pi conditions, the chloroplastic APX activities in WT and Rubisco-sense plants were activated compared to the control-Pi conditions, and showed similar values to that in Rubisco-antisense plants (Figure S3b, c). The total- and Cu/Zn-SOD activities were higher in the Rubisco-antisense plants than in the WT and Rubisco-sense plants under the control-Pi conditions (Figure S3d). However, under 3.0 mM-Pi conditions, the Cu/Zn-SOD activities in the Rubisco-antisense plants were suppressed similar to those in the WT and Rubisco-sense plants. These results indicated that the P toxicity-mediated suppression of photosynthesis triggers an increase in APX activity as similar to the results of the Rubisco-antisense plants, but the Cu/Zn-SOD activity showed different responses between excessive Pi treatments and a decrease in the Rubisco content, even though both situations limit photosynthesis.

Higher Pi application does not suppress all Cu/Zn-SOD mRNA expressions

Rice plants encode five Cu/Zn-SOD genes in their genomes (RiceXPro; http://ricexpro.dna.affrc.go.jp/). All mRNA expressions encoding Cu/Zn-SOD were determined on the leaf fresh weight and the 18S ribosome mRNA expression bases relative to those of the control-Pi plants respectively. The expression of *cytCu/ZnSOD1,2* and*CuZnSOD3* increased with increasing Pi application (Figure 6a-c), but those of *perCuZnSOD* and *chlCuZnSOD* were not affected by Pi application (Figure 6d, e). Thus, the responses of these mRNA expressions could not account for the decrease in Cu/Zn-SOD activity.

Excessive Pi application dose not inhibit other nutrient absorptions, but might decrease some nutrient availabilities

To investigate why Cu/Zn-SOD activity decreased in the higher-Pi treatments, the content of several essential nutrient elements was determined using the inductively coupled plasma atomic emission spectroscopy (ICP-AES). The P content increased with increasing Pi application (Figure 7a). The content values of K, Ca, and Fe were not affected by Pi application (Figure 7a), but those of Mg, Mn, Zn, and Cu increased with increasing Pi application (Figure 7a).

To deduce nutrient availabilities within leaves, we next examined the mRNA expressions of several metal deficiency-responsive genes, such as*ZIP4* (Ishimaru et al., 2005), *IRO2* (Ogo et al., 2006) and*COPT1* (Yuan et al., 2011), which are expressed under Zn-, Fe-, and Cu-deficient conditions, respectively. The *ZIP4* and*IRO2* expressions increased with increasing in Pi application (Figure 7b), *COPT1* expression showed no significant change with varying Pi application conditions (Figure 7b). These results suggest that excessive Pi application does not inhibit the metal transport to leaves, but Zn- and Fe-deficiency occurs within cells under conditions of excessive Pi application.

Phytic acid synthesis is upregulated by excessive Pi application

Mitsuhashi et al. (2005) reported that exposing the cultured cells of*Catharanthus roseus* and *Arabidopsis* to high Pi conditions stimulates phytic acid synthesis and accumulation phytic acid in both cytosol and vacuoles. Based on this observation, we examined whether high Pi accumulation stimulates phytic acid synthesis in leaves. Perera et al. (2018) summarized the putative genes involved in phytic acid synthesis in rice plants. Among those, we selected the genes that are expressed in leaves using the Rice-XPro data base and quantified their mRNA expressions. Figure 8a shows the phytic acid synthesis pathways as well as the genes involved in those pathways (Suzuki et al., 2007; Perera et al., 2018). The *INO1, IPK1, IPK2, 2-PGK, ITPK3-1, ITPK3-2, ITPK5,* and *ITPK6* transcript levels tended to increase with increasing in Pi application (Figure 8b). On the other hand, the*IMP1-1* transcript levels increased only under low-Pi conditions. The *IMP1-2* , *ITPK1,* and *ITPK2* transcript levels showed no clear response to the Pi application.

To certify that the change in mRNA expression of the genes involved in phytic acid synthesis actually changes the phytic acid content in leaves, we quantified the phytic acid content in leaves. The leaf phytic acid content was comparable between the low-Pi and control-Pi plants (Figure 8c, d). As with the increase in Pi application, the leaf phytic acid content increased and the 2.4 and 3.0 mM Pi plants showed significantly higher phytic acid content than the control-Pi plants (Figure 8c, d). Figure 8e shows the phytic acid/free Pi ratio in the leaves. Under 0.06 mM Pi conditions, the phytic acid/free Pi ratio was significantly higher than that under other Pi application conditions. In contrast, the increase in Pi application from the control-Pi to 3.0 mM Pi did not change the phytic acid/free Pi ratio in the leaves. These results indicated that the phytic acid content increases with increasing Pi content in the leaves of all Pi-treated plants, except for the low-Pi plants.

DISCUSSION

Owing to the low concentrations of Pi in the soil (< 10 μM) (Bieleski, 1973), Pi acquisition often limits plant growth and crop yield. For this reason, improving Pi absorption and utilization in land plants is one of the molecular targets for increasing agricultural productivity (Gu et al., 2016). On the other hand, excessive Pi absorption in plants causes P toxicity (Gu et al., 2016). Therefore, to improve Pi-use efficiency in crops, P toxicity must be avoided, and the mechanisms of P toxicity should be understood. However, the detailed mechanisms of illumination-dependent P toxicity that causes leaf withering in land plants remain to be clarified (Cakmak & Marscher, 1987; Delhaize & Randall, 1995; Ova et al., 2015). To address this question, we characterized the effects of different Pi application conditions on rice plants from the aspect of photosynthesis. Here, we propose three important factors underlying P toxicity symptoms: activation of the phytic acid synthesis pathway in the leaves, limitation of photosynthesis, and disruption of Cu/Zn-SOD activity.

We suggest that P toxicity is triggered by activating phytic-acid synthesis and decreasing metal availability in leaves. In seeds, phytic acid synthesis is stimulated in response to Pi accumulation for storing P and metals (Hawkesford et al., 2012; Su et al., 2018). In line with this observation, we found that phytic acid synthesis substantially occurs with an increase in Pi accumulation in the leaves due to the upregulation of the gene expressions involved in phytic acid synthesis (Table 1; Figure 8). The activation of phytic acid synthesis would be triggered by an increase in G6P content in the cytosol (Figure. 3b). Under higher Pi application conditions, the sugar-phosphate content increased in both chloroplasts and cytosols (Figure. 3b). The triose-phosphate translocator (TPT) exports 3-PGA and triose-phosphate between chloroplasts and cytosol by exchanging Pi (Flügge & Heldt, 1984). An increase in the cytosolic Pi level would stimulate the export of triose-phosphate from the chloroplasts to the cytosol (Flügge, 1992), and the metabolic flux involving sugar-phosphates (Figure 3a, b). The phytic-acid synthesis occurs by two distinct pathways, lipid-dependent and lipid-independent (Figure 8a) (Suzuki et al., 2007; Perera et al., 2018). The lipid-independent pathway responded to an increase in Pi accumulation in the leaves, and an increase in the phytic acid/free Pi ratio suggests that certain proportion of Pi is converted to phytic acid in accordance with the sugar-phosphate accumulation (Figure 3b; Figure 8b-e). Phytic acid has high metal-chelating activity, and Maenz et al. (1999) showed that Zn, rather than other metals, is an exclusive target of phytic acid. Thus, an increase in *ZIP4* expression suggests that phytic acid captures Zn within cells and insolubilizes it (Figure 7b). In fact, Cakmak and Marschner (1987) observed that Pi accumulation increased the insoluble Zn content in the leaves. Furthermore, the cytosolic pH (around 7.5) is optimal for phytic acid to chelate Zn (Maenz et al., 1999; Mimura et al., 2000). Previous studies showed that phytic acid is synthesized in the cytosol, and is stored in the vacuoles of the leaf cells (Mitsuhashi et al., 2005; Nagy et al., 2009; Lee et al., 2015). Moreover, the suppression of the Pi transport to vacuoles stimulates the P toxicity symptoms (Liu et al., 2015; Liu et al., 2016). Based on these studies, an increase in the cytosolic Pi accelerates triose phosphate export and G6P synthesis, thereby stimulating the synthesis of phytic acid, which, in turn, insolubilizes Zn in the cytosol. This can explain the previous observation of P toxicity symptoms similar to Zn deficiency symptoms in land plants, despite substantial accumulation of Zn in land plants (Cakmak & Marscher, 1987; Ova et al., 2015). In contrast to *ZIP4* , *COPT1* expression showed no significant response to an increase in Pi accumulation in the leaves, implying that a decrease in Cu/Zn-SOD activity was caused by the suppression of Zn availability in cells. Fe is also a target of phytic acid accumulation. In fact, *IRO2* expression increased with increasing Pi accumulation (Figure 7b) (Maenz et al., 1999). However, a decrease in Fe- and Mn-SOD activities was not found (Figure 5c). APX also contains Fe as a co-factor, and its activity decreased under Fe-deficiency conditions (Ranieri et al., 2001). However, the APX activity was rather increased under high-Pi conditions (Figure 5a, b and Figure S3b, c). These results suggest that Fe-deficiency is not severe than Zn-deficiency within cells under P toxicity conditions. Interestingly, *IMP1-1* expression was activated under low-Pi conditions (Figure 8b). The phytic acid/free Pi ratio showed a response similar to that of *IMP1-1* expression (Figure 8e). These results suggest that the lipid-dependent phytic acid synthesis pathway could be activated under low-Pi conditions. Although phytic acid is a major storage-form of Pi in seeds (Hawkesford et al., 2012), the inhibition of phytic acid synthesis led to leaf morphology distortion in *Arabidopsis* or growth retardation in crop plants (Raboy et al., 2000; Stevenson-Paulik et al., 2005). Lee et al. (2015) demonstrated that phytic acid is required for activating LOS4/Gle1-mediated mRNA export from nucleus in *Arabidopsis* in a manner similar to animals and yeast, and the phytic acid deficiency causes mRNA accumulation within nuclei. In addition, phytic acid inactivates inward K^+ conductance by mobilizing Ca^{2+} in the plasma membranes in response to abscisic acid in the guard cells and contributes to pathogen defense (Lemtiri-Chlieh et al., 2000, 2003; Murphy et al., 2008; Nagy et al., 2009). Based on these studies, the lipid-dependent pathway might secure phytic acid synthesis under low-Pi availability conditions to maintain the phytic acid dependent physiological reactions. Further investigation is required to elucidate the validity of this hypothesis.

The limitation of photosynthesis would be enhanced by a decrease in the RCA content. We found that Pi accumulation decreases electron sink capacities by deactivating Rubisco, but not lowering Rubisco content (Figures 2 and 4). Furthermore, the α - and β -forms of RCA were significantly decreased with an increase in Pi application (Figure 4e-i). Among the three RCA iso-forms, the α - and β -forms are the major components

of Rubisco activation (Zhang et al., 2002; Portis, 2003), and it has not been addressed whether the β^* -form has the ability to activate Rubisco. These results suggest that the target of P toxicity exists not in Rubisco itself, but within the isoforms of RCA, especially α - and β -forms. In the RCA mutants of *Arabidopsis* and rice plants, A linearly increases with increasing Ci in a manner similar to our results under high Pi conditions in WT plants (Zhang et al., 2002; Masumoto et al., 2012; Yamori et al., 2012). Although we could not elucidate the detailed mechanism to differentiate the content of RCA isoforms in the leaves, Vargas-Suárez et al. (2004) suggested that the β^* -form is generated by limited proteolysis under stress conditions, such as drought, and changing the β- form to β^*- form resulted in higher chaperone activity. From this point, we suggest the possibility that the β^* -form is upregulated to protect proteins under the oxidative stress conditions caused by P toxicity at the cost of Rubisco activation. Supporting this idea, Rokka et al. (2001) suggested that RCA plays a second role as a chaperone for protecting thylakoid membrane proteins under heat stress conditions, that is, the physiological functions of RCA would not be limited to activate Rubisco.

We suggest that the severe limitation of photosynthesis is caused by additional factors in concert with a decrease in the RCA content. Badger & Lorimer (1981) reported that Pi acts as a weak Rubisco inhibitor*in vitro* , that is, Rubisco activation might be further declined under P toxicity conditions *in vivo* . Moreover, Suzuki et al. (2012) reported that when Rubisco severely limits the photosynthetic metabolic flux in the leaves, the RuBP content is increased. Here, we observed that an increase in the sugar-phosphate content of the latter part of GA3P and DHAP rather than an increase in RuBP (Figure 3b). This result suggested that another target, besides RCA, should be suppressed under P toxicity conditions.

Under P toxicity conditions, leaf withering would be caused by the oxidative stress resulting from the disruption of Cu/Zn-SOD activities as well as photosynthetic limitation. When PET activity exceeds the electron sink capacity, ROS production is stimulated in both PSII and PSI (Krieger-Liszkay, 2005; Sonoike, 2011; Pospíšil, 2016; Takagi et al., 2016a). ROS show high reactivity to biomolecules including DNA, proteins and lipids; therefore, the accumulation of ROS triggers cellular dysfunction to cause cell death (Apel & Hirt, 2004). Under high-Pi conditions, an increase was observed in the values of Y(NO) and Y(NA), which indicate the reduced states of PSII and PSI, respectively, despite an increase in the values of NPQ and Y(ND), which contribute to the suppression of ROS production both in PSII and PSI (Figure 2; Figures S1) (Müller et al., 2001; Takagi et al., 2017). Wada et al. (2018) reported that the Rubisco-antisense plants showed an over-reduction of the PET chain. Furthermore, Takagi et al. (2016b) reported that the suppression of electron sink activities inhibits both PET reaction andpmf generation. At the same time, the values of $g_H{}^+$ and$V_H{}^+$ also decreased because of the decrease in the ATP requirement of electron sink activities (Takagi et al., 2016b). Here, we observed that the ATP/ADP ratio significantly increased with increaseing Pi application (Figure 3d). Moreover,pmf , $g_H{}^+$, and$V_H{}^+$ decreased under 3.0 mM Pi conditions (Figure S2). Therefore, the high Pi accumulation would cause an over-reduction of the PET chain owing to a decrease in electron sink activities, including Rubisco deactivation. An increase in APX activity reconciles with the stimulation of oxidative stress under P toxicity conditions because the chloroplastic APX activity responds to the oxidative stress (Figure 5a, b) (Cakmak, 2005). Furthermore, a decrease in the Chl content which with the decreasing in PSI (Figure 1c; Figure S4), and the decrease in Fv/Fm supports the oxidative stress on the thylakoid membranes under excessive Pi application conditions (Figure 2j) (Terashima et al., 1994; Sonoike, 2011; Takagi et al., 2016a). In addition, we found an increase in the expression of an ROS-responsive gene *PR5* (Ganesan & Thomas, 2001), and lipid hydroperoxide content (LOOH) under high-Pi application conditions (Figure S5a, c). In contrast, the expression of a programmed cell death-related gene *VPE2* (Deng et al., 2011) decreased under high-Pi conditions (Figure S5b). Based on the illumination dependency of P toxicity symptoms (Delhaize & Randall, 1995), necrosis but not programmed cell death would be triggered by ROS production in thylakoid membranes, and this would be intensified by both the suppression of Cu/Zn-SOD activity and a decrease in photosynthetic electron sink capacities (Figure 9).

In the present study, we discussed a detailed mechanism for P toxicity in rice plants (Figure 9). To date, much attention has been paid to phytic acid synthesis in seeds. However, our results indicated that to maintain a proper leaf phytic acid content is important for maintaining plant growth and escaping oxidative stress triggered by PET reaction. Because the phytic acid synthesis pathway would be activated by an

increase in the cytosolic Pi content through an increase in the sugar-phosphate content, the fine-tuning of Pi compartmentation within cells or modulation of sugar-phosphate metabolic flux might contribute to improving the Pi-use efficiency in the absence of phytic acid synthesis and P toxicity symptoms. The present study would open new opportunity to design breeding strategies for improving P use efficiency in crop plants. To modify the phytic acid content in land plants is also an important goal to improve human health because of severe Zn and Fe deficiency of humans in the world (Perera et al., 2018). That is, our findings would contribute to minimizing the phytic acid content as well as maximizing the plant yield for improving human health, especially for overcoming Zn-deficiency in humans and for fulfilling food demands in the future. Based on the present knowledge, we must continue to challenge ourselves to achieve these two important subjects in the main crop.

REFERENCE

Amako, K., Chen, G.X. & Asada, K. (1994). Separate assays specific for ascorbate peroxidase and guaiacol peroxidase and for the chloroplastic and cytosolic isozymes of ascorbate peroxidase in plants. *Plant and Cell Physiology,* 35(3), 497-504.

Apel, K. & Hirt, H. (2004). Reactive oxygen species: metabolism, oxidative stress, and signal transduction. *Annual Review of Plant Biology* , 55, 373-399.

Aung, K., Lin, S.I., Wu, C.C., Huang, Y.T., Su, C.L., & Chiou, T.J. (2006). *pho2* , a phosphate overaccumulator, is caused by a nonsense mutation in a microRNA399 target gene. *Plant Physiology* , 141(3), 1000-1011.

Badger, M.R. & Lorimer, G.H. (1981). Interaction of sugar phosphates with the catalytic site of ribulose-1, 5-bisphosphate carboxylase. *Biochemistry* , 20(8), 2219-2225.

Baker, N.R. (2008). Chlorophyll fluorescence: a probe of photosynthesis in vivo. *Annual Review of Plant Biology* , *59* , 89-113.

Bari, R., Pant, B.D., Stitt, M. & Scheible, W.R. (2006). PHO2, microRNA399, and PHR1 define a phosphate-signaling pathway in plants. *Plant Physiology.,* 141(3), 988-999.

Bhatti, A.S. & Loneragan, J.F. (1970). The effect of early superphosphate toxicity on the subsequent growth of wheat. *Australian Journal of Agricultural Research,* 21(6), 881-892.

Biddulph, O., Biddulph, S., Cory, R. & Koontz, H. (1958). Circulation patterns for phosphorus, sulfur and calcium in the bean plant. *Plant Physiology* , 33(4), 293-300.

Bieleski, R.L. (1973). Phosphate pools, phosphate transport, and phosphate availability. *Annual Reveiw of Plant Physiology,* 24, 225-252.

Cakmak, I. (2005). The role of potassium in alleviating detrimental effects of abiotic stresses in plants. *Journal of Plant Nutrition and Soil Science,* 168(4), 521-530.

Cakmak, I. & Marschner, H. (1987). Mechanism of phosphorus-induced zinc deficiency in cotton. III. Changes in physiological availability of zinc in plants Is mail. *Physiologia Plantarum* , 70(1), 13-20.

Cheng, Y., Zhou, W., El Sheery, N.I., Peters, C., Li, M., Wang, X. & Huang, J. (2011). Characterization of the Arabidopsis glycerophosphodiester phosphodiesterase (GDPD) family reveals a role of the plastid-localized AtGDPD1 in maintaining cellular phosphate homeostasis under phosphate starvation. *The Plant Journal* , 66(5), 781-795.

Chiou, T.J., Aung, K., Lin, S.I., Wu, C.C., Chiang, S.F. & Su, C.L. (2006). Regulation of phosphate homeostasis by microRNA in*Arabidopsis* . *The Plant Cell* , 18(2), 412-421.

Clarkson, D.T. & Scattergood, C.B. (1982). Growth and phosphate transport in barley and tomato plants during the development of, and recovery from, phosphate-stress. *Journal of Experimental Botany,* 33(5), 865-875.

Delhaize, E. & Randall, P.J. (1995). Characterization of a phosphate-accumulator mutant of Arabidopsis thaliana. *Plant Physiology.* , 107(1), 207-213.

Deng, M., Bian, H., Xie, Y., Kim, Y., Wang, W., Lin, E., Zeng, Z., Guo, F., Pan, J., Han, N., Wang, J., Qian, Q. & Zhu, M. (2011). Bcl-2 suppresses hydrogen peroxide-induced programmed cell death via *OsVPE2* and *OsVPE3* , but not via *OsVPE1* and *OsVPE4* , in rice. *The FEBS Journal,* 278(24), 4797-4810.

Dong, B., Rengel, Z. & Delhaize, E. (1998). Uptake and translocation of phosphate by pho2 mutant and wild-type seedlings of *Arabidopsis thaliana.* *Planta* , 205(2), 251-256.

Fabre, D., Yin, X., Dingkuhn, M., Clement-Vidal, A., Roques, S., Rouan, L., Soutiras, A. & Luquet, D. (2019). Is triose phosphate utilization involved in the feedback inhibition of photosynthesis in rice under conditions of sink limitation? *Journal of Experimental Botany* , 70(20), 5773-5785.

Flohe, L. & Otting, F. (1984). Superoxide dismutase assays. In Methods in enzymology (eds L. Packer), Vol. 105, pp. 93-104, Academic Press, Orlando.

Flugge, U.I. (1992). Reaction mechanism and asymmetric orientation of the reconstituted chloroplast phosphate translocator. *Biochim Biophys Acta Biomembranes* , 1110(1), 112-118.

Flugge, U.I. & Heldt, H.W. (1984). The phosphate-triose phosphate-phosphoglycerate translocator of the chloroplast. *Trends in Biochemical Sciences,* 9(12), 530-533.

Franco-Zorrilla, J.M., Valli, A., Todesco, M., Mateos, I., Puga, M.I., Rubio-Somoza, I., Leyva, A., Weigel, D., Garcia, J.A. & Paz-Ares, J. (2007). Target mimicry provides a new mechanism for regulation of microRNA activity. *Nature Genetics* , 39(8), 1033-1037.

Fujii, H., Chiou, T.J., Lin, S.I., Aung, K., and Zhu, J.K. (2005). A miRNA involved in phosphate-starvation response in*Arabidopsis* . *Current Biology* , 15(22), 2038-2043.

Fukayama, H., Ueguchi, C., Nishikawa, K., Katoh, N., Ishikawa, C., Masumoto, C., Hatanaka, T. & Misoo, S. (2012). Overexpression of Rubisco activase decreases the photosynthetic CO_2assimilation rate by reducing Rubisco content in rice leaves.*Plant Cell Physiology,* 53(6), 976-986.

Furihata, T., Suzuki, M. & Sakurai, H. (1992). Kinetic characterization of two phosphate uptake systems with different affinities in suspension-cultured *Catharanthus roseus* protoplasts. *Plant and Cell Physiology* , 33(8), 1151-1157.

Ganesan, V. & Thomas, G. (2001). Salicylic acid response in rice: influence of salicylic acid on H_2O_2accumulation and oxidative stress. *Plant Science* , 160(6), 1095-1106.

Gu, M., Chen, A., Sun, S. & Xu, G. (2016). Complex regulation of plant phosphate transporters and the gap between molecular mechanisms and practical application: what is missing? *Molecular Plant* , 9(3), 396-416.

Hawkesford, M., Horst, W., Kichey, T., Lambers, H., Schjoerring, J., Moller, I.S. & White, P. (2012). Functions of macronutrients. In *Marschner's mineral nutrition of higher plants* (eds Marschner, P.), pp. 135-189. Academic Press, London.

Ishimaru, Y., Suzuki, M., Kobayashi, T., Takahashi, M., Nakanishi, H., Mori, S. & Nishizawa, N.K. (2005). OsZIP4, a novel zinc-regulated zinc transporter in rice. *Journal of Experimental Botany* , 56(422), 3207-3214.

Kai, M., Masuda, Y., Kikuchi, Y., Osaki, M. & Tadano, T. (1997). Isolation and characterization of a cDNA from *Catharanthus roseus*which is highly homologous with phosphate transporter. *Soil Science and Plant Nutrition* , 43(1), 227-235.

Kirkby, E. (2012). Introduction, definition and classification of nutrients. In *Marschner's Mineral Nutrition of Higher Plants* (eds Marschner, P.) (pp. 3-5). Academic Press. London.

Klughammer, C. & Schreiber, U. (1994). An improved method, using saturating light pulses, for the determination of photosystem I quantum yield via $P700^{+}$-absorbance changes at 830 nm. *Planta* , 192(2), 261-268.

Kramer, D.M., Johnson, G., Kiirats, O. & Edwards, G.E. (2004). New fluorescence parameters for the determination of $Q_A$redox state and excitation energy fluxes. *Photosynthesis Reserch,*79(2), 209-218.

Krieger-Liszkay, A. (2005). Singlet oxygen production in photosynthesis.*Journal of Experimental Botany* , 56(411), 337-346.

Kurita, Y., Baba, K.I., Ohnishi, M., Anegawa, A., Shichijo, C., Kosuge, K., Fukaki, H. & Mimura, T. (2014). Establishment of a shortened annual cycle system; a tool for the analysis of annual re-translocation of phosphorus in the deciduous woody plant (*Populus alba* L.).*Journal of Plant Reserch* , 127(4), 545-551.

Lee, H. S., Lee, D.H., Cho, H.K., Kim, S.H., Auh, J.H. & Pai, H.S. (2015). InsP6-sensitive variants of the Gle1 mRNA export factor rescue growth and fertility defects of the *ipk1* low-phytic-acid mutation in *Arabidopsis* . *The Plant Cell* , 27(2), 417-431.

Lee, R.B., Ratcliffe, R.G., & Southon, T.E. (1990).^{31}P NMR measurements of the cytoplasmic and vacuolar Pi content of mature maize roots: relationships with phosphorus status and phosphate fluxes. *Journal of Experimental Botany* , 41(9),: 1063-1078.

Leggewie, G., Willmitzer, L. & Riesmeier, J.W. (1997). Two cDNAs from potato are able to complement a phosphate uptake-deficient yeast mutant: identification of phosphate transporters from higher plants. *The Plant Cell* , 9(3), 381-392.

Lemtiri-Chlieh, F., MacRobbie, E.A. & Brearley, C.A. (2000). Inositol hexakisphosphate is a physiological signal regulating the K^{+}-inward rectifying conductance in guard cells.*Proceedings of the National Academy of Sciences,* 97(15), 8687-8692.

Lemtiri-Chlieh, F., MacRobbie, E.A., Webb, A.A., Manison, N.F., Brownlee, C., Skepper, J.N., Chen, J., Prestwich, G.D. & Brearley, C.A. (2003). Inositol hexakisphosphate mobilizes an endomembrane store of calcium in guard cells. *Proceedings of the National Academy of Sciences,* 100(17), 10091-10095.

Lin, S.I., Santi, C., Jobet, E., Lacut, E., El Kholti, N., Karlowski, W.M., Verdeil, J.L., Breitler, J.C., Perin, C., Ko, S.S., Guiderdoni, E., Chiou, T.J. & Guiderdoni, E. (2010). Complex regulation of two target genes encoding SPX-MFS proteins by rice miR827 in response to phosphate starvation. *Plant and Cell Physiology,* 51(12), 2119-2131.

Liu, C., Muchhal, U.S., Uthappa, M., Kononowicz, A.K. & Raghothama, K.G. (1998). Tomato phosphate transporter genes are differentially regulated in plant tissues by phosphorus. *Plant Physiology* , 116(1), 91-99.

Liu, F., Wang, Z., Ren, H., Shen, C., Li, Y., Ling, H. Q., Wu, C., Lian, X. & Wu, P. (2010). OsSPX1 suppresses the function of OsPHR2 in the regulation of expression of *OsPT2* and phosphate homeostasis in shoots of rice. The *Plant Journal* , 62(3), 508-517.

Liu, J., Yang, L., Luan, M., Wang, Y., Zhang, C., Zhang, B., Shi, J., Zhao, F.G., Lan, W. & Luan, S. (2015). A vacuolar phosphate transporter essential for phosphate homeostasis in *Arabidopsis* .*Proceedings of the National Academy of Sciences* , 112(47), E6571-E6578.

Liu, T.Y., Huang, T.K., Yang, S.Y., Hong, Y.T., Huang, S.M., Wang, F.N., Chiang, S.F., Tsai, S. Y., Lu, W.C. & Chiou, T.J. (2016). Identification of plant vacuolar transporters mediating phosphate storage. *Nature Communications,* doi:10.1038/ncomms11095.

Loneragan, J.F., Grove, T.S., Robson, A.D. & Snowball, K. (1979). Phosphorus Toxicity as a Factor in Zinc-Phosphorus Interactions in Plants 1. *Soil Science Society of America Journal,* 43(5), 966-972.

Maenz, D.D., Engele-Schaan, C.M., Newkirk, R.W. & Classen, H.L. (1999). The effect of minerals and mineral chelators on the formation of phytase-resistant and phytase-susceptible forms of phytic acid in

solution and in a slurry of canola meal. *Animal Feed Science and Technology,* 81(3-4), 177-192.

Makino, A., Mae, T. & Ohira, K. (1986). Colorimetric measurement of protein stained with Coomassie Brilliant Blue R on sodium dodecyl sulfate-polyacrylamide gel electrophoresis by eluting with formamide. *Agricultural and Biological Chemistry,* 50(7), 1911-1912.

Makino, A., Nakano, H. & Mae, T. (1994). Responses of ribulose-1, 5-bisphosphate carboxylase, cytochrome f, and sucrose synthesis enzymes in rice leaves to leaf nitrogen and their relationships to photosynthesis. *Plant Physiology* , 105(1), 173-179.

Makino, A., Nakano, H., Mae, T., Shimada, T. & Yamamoto, N. (2000). Photosynthesis, plant growth and N allocation in transgenic rice plants with decreased Rubisco under CO_2enrichment. *Journal of Experimental Botany* , 51(suppl_1), 383-389.

Masumoto, C., Fukayama, H., Hatanaka, T. & Uchida, N. (2012). Photosynthetic characteristics of antisense transgenic rice expressing reduced levels of Rubisco activase. *Plant Production Science,*15(3), 174-182.

Mekawy, A.M.M., Assaha, D.V., Munehiro, R., Kohnishi, E., Nagaoka, T., Ueda, A. & Saneoka, H. (2018). Characterization of type 3 metallothionein-like gene (OsMT-3a) from rice, revealed its ability to confer tolerance to salinity and heavy metal stresses.*Environmental and Experimental Botany* , 147, 157-166.

Mimura, T. (1995). Homeostasis and transport of inorganic phosphate in plants. *Plant and Cell Physiology* , 36(1), 1-7.

Mimura, T. (1999). Regulation of phosphate transport and homeostasis in plant cells. In *International Review of Cytology* (eds Kwang W. Jeon.), Vol. 191, pp. 149-200, Academic Press, New York.

Mimura, T., Dietz, K.J., Kaiser, W., Schramm, M.J., Kaiser, G. & Heber, U. (1990). Phosphate transport across biomembranes and cytosolic phosphate homeostasis in barley leaves. *Planta* , 180(2), 139-146.

Mimura, T., Sakano, K. & Shimmen, T. (1996). Studies on the distribution, re-translocation and homeostasis of inorganic phosphate in barley leaves. *Plant, Cell and Environment* , 19(3), 311-320.

Mimura, T., Shindo, C., Kato, M., Yokota, E., Sakano, K., Ashihara, H. & Shimmen, T. (2000). Regulation of cytoplasmic pH under extreme acid conditions in suspension cultured cells of *Catharanthus roseus* : a possible role of inorganic phosphate. *Plant and Cell Physiology* , 41(4), 424-431.

Mimura, T., Yin, Z. H., Wirth, E. & Dietz, K.J. (1992). Phosphate transport and apoplastic phosphate homeostasis in barley leaves. *Plant and Cell Physiology* , 33(5), 563-568.

Mitsuhashi, N., Ohnishi, M., Sekiguchi, Y., Kwon, Y.U., Chang, Y.T., Chung, S.K., Inoue, Y., Reid, R.J., Yagisawa, H. & Mimura, T. (2005). Phytic acid synthesis and vacuolar accumulation in suspension-cultured cells of *Catharanthus roseus* induced by high concentration of inorganic phosphate and cations. *Plant Physiology* , 138(3), 1607-1614.

Miyagi, A., Takahashi, H., Takahara, K., Hirabayashi, T., Nishimura, Y., Tezuka, T., Kawai-Yamada, M. & Uchimiya, H. (2010). Principal component and hierarchical clustering analysis of metabolites in destructive weeds; polygonaceous plants. *Metabolomics,* 6(1), 146-155.

Miyagi, A., Noguchi, K., Tokida, T., Usui, Y., Nakamura, H., Sakai, H., Hasegawa, T. & Kawai-Yamada, M. (2019). Oxalate contents in leaves of two rice cultivars grown at a free-air CO_2 enrichment (FACE) site. *Plant Production Science,* 22, 407-411.

Muchhal, U.S., Pardo, J.M. & Raghothama, K.G. (1996). Phosphate transporters from the higher plant *Arabidopsis thaliana* .*Proceedings of the National Academy of Sciences* , 93(19), 10519-10523.

Murphy, A.M., Otto, B., Brearley, C.A., Carr, J.P. & Hanke, D.E. (2008). A role for inositol hexakisphosphate in the maintenance of basal resistance to plant pathogens. *The Plant Journal* , 56(4), 638-652.

Muller, P., Li, X.P., & Niyogi, K.K. (2001). Non-photochemical quenching. A response to excess light energy. *Plant Physiology* , 125(4), 1558-1566.

Nagy, R., Grob, H., Weder, B., Green, P., Klein, M., Frelet-Barrand, A., Schjoerring J.K., Brearley, C. & Martinoia, E. (2009). The Arabidopsis ATP-binding cassette protein AtMRP5/AtABCC5 is a high affinity inositol hexakisphosphate transporter involved in guard cell signaling and phytate storage. *Journal of Biological Chemistry,* 284(48), 33614-33622.

Nakamura, Y. (2013). Phosphate starvation and membrane lipid remodeling in seed plants. *Progress in Lipid Research,* 52(1), 43-50.

Noguchi, K., Tsunoda, T., Miyagi, A., Kawai-Yamada, M., Sugiura, D., Miyazawa, S. I., Tokida, T., Usui, Y., Nakamura, H., Sakai, H. & Hasegawa, T. (2018). Effects of elevated atmospheric CO_2on respiratory rates in mature leaves of two rice cultivars grown at a free-air CO_2 enrichment site and analyses of the underlying mechanisms. *Plant and Cell Physiology,* 59(3), 637-649.

Nussaume, L., Kanno, S., Javot, H., Marin, E., Nakanishi, T.M. & Thibaud, M.C. (2011). Phosphate import in plants: focus on the PHT1 transporters. *Frontiers in Plant Science,* 2:83. doi: 10.3389/fpls.2011.00083.

Ogawa, S., Suzuki, Y., Yoshizawa, R., Kanno, K. & Makino, A. (2012). Effect of individual suppression of RBCS multigene family on Rubisco contents in rice leaves. *Plant, Cell and Environment,* 35(3), 546-553.

Ogo, Y., Itai, R.N., Nakanishi, H., Inoue, H., Kobayashi, T., Suzuki, M., Takahashi, M., Mori, S. & Nishizawa, N.K. (2006). Isolation and characterization of IRO2, a novel iron-regulated bHLH transcription factor in graminaceous plants. *Journal of Experimental Botany,*57(11), 2867-2878.

Ova, E.A., Kutman, U.B., Ozturk,L. & Cakmak, I. (2015). High phosphorus supply reduced zinc concentration of wheat in native soil but not in autoclaved soil or nutrient solution. *Plant and Soil,* 393(1-2), 147-162.

Perera, I., Fukushima, A., Arai, M., Yamada, K., Nagasaka, S., Seneweera, S. & Hirotsu, N. (2019). Identification of low phytic acid and high Zn bioavailable rice (*Oryza sativa* L.) from 69 accessions of the world rice core collection. *Journal of Cereal Science,* 85, 206-213.

Perera, I., Seneweera, S., & Hirotsu, N. (2018). Manipulating the Phytic Acid Content of Rice Grain Toward Improving Micronutrient Bioavailability. *Rice* , 11(1), 4.

Porra, R.J., Thompson, W.A. & Kriedemann, P.E. (1989). Determination of accurate extinction coefficients and simultaneous equations for assaying chlorophylls *a* and *b* extracted with four different solvents: verification of the concentration of chlorophyll standards by atomic absorption spectroscopy. *Biochimica et Biophysica Acta -Bioenergetics,* 975(3), 384-394.

Portis, A.R. (2003). Rubisco activase–Rubisco's catalytic chaperone.*Photosynthesis research,* 75(1), 11-27.

Pospišil, P. (2016). Production of reactive oxygen species by photosystem II as a response to light and temperature stress.*Frontiers in Plant Science,* 7:1950. doi: 10.3389/fpls.2016.01950.

Pratt, J., Boisson, A.M., Gout, E., Bligny, R., Douce, R. & Aubert, S. (2009). Phosphate (Pi) starvation effect on the cytosolic Pi concentration and Pi exchanges across the tonoplast in plant cells: an in vivo 31P-nuclear magnetic resonance study using methylphosphonate as a Pi analog. *Plant Physiology,* 151(3), 1646-1657.

Puga, M.I., Mateos, I., Charukesi, R., Wang, Z., Franco-Zorrilla, J.M., de Lorenzo, L., Irigoyen, M.L., Masiero, S., Bustos, R., Rodriguez, J., Leyva, A., Rubio, V., Sommer, H. & Leyva, A. (2014). SPX1 is a phosphate-dependent inhibitor of Phosphate Starvation Response 1 in*Arabidopsis* . *Proceedings of the National Academy of Sciences* , 111(41), 14947-14952.

Raboy, V., Gerbasi, P.F., Young, K.A., Stoneberg, S.D., Pickett, S.G., Bauman, A.T., Murthy, P.P., Sheridan, W.F. & Ertl, D.S. (2000). Origin and seed phenotype of maize low phytic acid 1-1 and low phytic acid

2-1.*Plant Physiology,* 124(1), 355-368.

Raghothama, K.G. (1999). Phosphate acquisition. *Annual Review of Plant Biology* , 50, 665-693.

Ranieri, A., Castagna, A., Baldan, B. & Soldatini, G.F. (2001). Iron deficiency differently affects peroxidase isoforms in sunflower.*Journal of Experimental Botany* , 52(354), 25-35.

Rossiter, R.C. (1951). Phosphorus toxicity in subterranean clover and oats grown on Muchea sand, and the modifying effects of lime and nitrate-nitrogen. *Australian Journal of Agricultural Research,*3(3), 227-243.

Rubio, V., Linhares, F., Solano, R., Martín, A.C., Iglesias, J., Leyva, A. & Paz-Ares, J. (2001). A conserved MYB transcription factor involved in phosphate starvation signaling both in vascular plants and in unicellular algae. *Genes and Development,* 15(16), 2122-2133.

Rokka, A., Zhang, L. & Aro, E.M. (2001). Rubisco activase: an enzyme with a temperature-dependent dual function?. *The Plant Journal,*25(4), 463-471.

Sacksteder, C. A. & Kramer, D.M. (2000). Dark-interval relaxation kinetics (DIRK) of absorbance changes as a quantitative probe of steady-state electron transfer. *Photosynthesis Research* , 66(1-2), 145-158.

Sakano, K. (1990). Proton/phosphate stoichiometry in uptake of inorganic phosphate by cultured cells of *Catharanthus roseus* (L.) G. Don.*Plant Physiology,* 93(2), 479-483.

Salvucci, M.E., Portis, A.R. & Ogren, W.L. (1985). A soluble chloroplast protein catalyzes ribulosebisphosphate carboxylase/oxygenase activation in vivo. *Photosynthesis Research,* 7(2), 193-201.

Secco, D., Wang, C., Arpat, B.A., Wang, Z., Poirier, Y., Tyerman, S.D., Wu, P., Shou, H. & Whelan, J. (2012). The emerging importance of the SPX domain-containing proteins in phosphate homeostasis. *New Phytologist,* 193(4), 842-851.

Sharkey, T.D. (1985). Photosynthesis in intact leaves of C3 plants: physics, physiology and rate limitations. *The Botanical Review* , 51(1), 53-105.

Shive, J.W. (1918). Toxicity of monobasic phosphates towards soybeans grown in soil-and solution-cultures. *Soil Science* , 5, 87-122.

Singh, J.P., Karamanos, R.E. & Stewart, J.W.B. (1988). The mechanism of phosphorus-induced zinc deficiency in bean (*Phaseolus vulgaris*L.). *Canadian Journal of Soil Science,* 68(2), 345-358.

Sonoike, K. (2011). Photoinhibition of photosystem I. *Physiologia. Plantarum* , 142(1), 56-64.

Su, D., Zhou, L., Zhao, Q., Pan, G. & Cheng, F. (2018). Different phosphorus supplies altered the accumulations and quantitative distributions of phytic acid, zinc, and iron in rice (*Oryza sativa* L.) Grains. *Journal of Agricultural and Food Chemistry,*66(7), 1601-1611.

Suganami, M., Suzuki, Y., Sato, T. & Makino, A. (2018). Relationship between Rubisco activase and Rubisco contents in transgenic rice plants with overproduced or decreased Rubisco content. *Soil Science and Plant Nutrition,* 64(3), 352-359.

Suzuki, M., Tanaka, K., Kuwano, M. & Yoshida, K.T. (2007). Expression pattern of inositol phosphate-related enzymes in rice (*Oryza sativa* L.): implications for the phytic acid biosynthetic pathway. *Gene* , 405(1-2), 55-64.

Suzuki, Y., Fujimori, T., Kanno, K., Sasaki, A., Ohashi, Y. & Makino, A. (2012). Metabolome analysis of photosynthesis and the related primary metabolites in the leaves of transgenic rice plants with increased or decreased Rubisco content. *Plant, Cell & Environment,* 35(8), 1369-1379.

Suzuki Y, Kawazu T. & Koyama, H. (2004). RNA isolation from siliques, dry seeds and other tissues of *Arabidopsis thaliana* .*Biotechniques,* 37(4), 542-544.

Suzuki, Y., Ohkubo, M., Hatakeyama, H., Ohashi, K., Yoshizawa, R., Kojima, S., Hayakawa, T., Yamaya, T., Mae, T. & Makino, A. (2007). Increased Rubisco content in transgenic rice transformed with the 'sense'rbcS gene. *Plant and Cell Physiology,* 48(4), 626-637.

Stevenson-Paulik, J., Bastidas, R.J., Chiou, S.T., Frye, R.A. & York, J.D. (2005). Generation of phytate-free seeds in *Arabidopsis*through disruption of inositol polyphosphate kinases. *Proceedings of the National Academy of Sciences,* 102(35), 12612-12617.

Takagi, D., Amako, K., Hashiguchi, M., Fukaki, H., Ishizaki, K., Goh, T., Fukao, Y., Sano, R., Kurata, T., Demura, T., Sawa, S. & Miyake, C. (2017). Chloroplastic ATP synthase builds up a proton motive force preventing production of reactive oxygen species in photosystem I.*The Plant Journal,* 91(2), 306-324.

Takagi, D., Hashiguchi, M., Sejima, T., Makino, A. & Miyake, C. (2016b). Photorespiration provides the chance of cyclic electron flow to operate for the redox-regulation of P700 in photosynthetic electron transport system of sunflower leaves. *Photosynthesis Research,*129(3), 279-290.

Takagi, D., Ihara, H., Takumi, S. & Miyake, C. (2019). Growth light environment changes the sensitivity of photosystem I photoinhibition depending on common wheat cultivars. *Frontiers in Plant Science,*10:686. doi: 10.3389/fpls.2019.00686.

Takagi, D., Takumi, S., Hashiguchi, M., Sejima, T. & Miyake, C. (2016a). Superoxide and singlet oxygen produced within the thylakoid membranes both cause photosystem I photoinhibition. *Plant Physiology* , 171(3), 1626-1634.

Terashima, I., Funayama, S. & Sonoike, K. (1994). The site of photoinhibition in leaves of Cucumis sativus L. at low temperatures is photosystem I, not photosystem II. *Planta,* 193(2), 300-306.

Ullrich-Eberius, C.I., Novacky, A., Fischer, E. & Luttge, U. (1981). Relationship between energy-dependent phosphate uptake and the electrical membrane potential in *Lemna gibba* G1. *Plant Physiology,* 67(4), 797-801.

Ullrich-Eberius, C.I., Novacky, A. & Van Bel, A.J.E. (1984). Phosphate uptake in *Lemna gibba* G1: energetics and kinetics. *Planta* ,*161* (1), 46-52.

Vargas-Suarez, M., Ayala-Ochoa, A., Lozano-Franco, J., Garcia-Torres, I., Diaz-Quinonez, A., Ortiz-Navarrete, V.F. & Sanchez-de-Jimenez, E. (2004). Rubisco activase chaperone activity is regulated by a post-translational mechanism in maize leaves. *Journal of Experimental Botany,* 55(408), 2533-2539.

von Caemmerer, S.V., & Farquhar, G.D. (1981). Some relationships between the biochemistry of photosynthesis and the gas exchange of leaves. *Planta* , 153(4), 376-387.

Wada, S., Suzuki, Y., Takagi, D., Miyake, C. & Makino, A. (2018). Effects of genetic manipulation of the activity of photorespiration on the redox state of photosystem I and its robustness against excess light stress under CO_2-limited conditions in rice.*Photosynthesis Research* , 137(3), 431-441.

Wang, C., Ying, S., Huang, H., Li, K., Wu, P. & Shou, H. (2009). Involvement of *OsSPX1* in phosphate homeostasis in rice. *The Plant Journal* , 57(5), 895-904.

Wang, Z., Ruan, W., Shi, J., Zhang, L., Xiang, D., Yang, C., Li, C., Wu, Z., Liu, Y., Shou, H., Mo, X., Mao, C. & Shou, H. (2014). Rice SPX1 and SPX2 inhibit phosphate starvation responses through interacting with PHR2 in a phosphate-dependent manner. *Proceedings of the National Academy of Sciences* , 111(41), 14953-14958.

Yamori, W., Masumoto, C., Fukayama, H. & Makino, A. (2012). Rubisco activase is a key regulator of non-steady-state photosynthesis at any leaf temperature and, to a lesser extent, of steady-state photosynthesis at high temperature. *The Plant Journal* , 71(6), 871-880.

Yuan, M., Li, X., Xiao, J. & Wang, S. (2011). Molecular and functional analyses of COPT/Ctr-type copper transporter-like gene family in rice. *BMC Plant Biology* , 11: 69. doi: 10.1186/1471-2229-11-69.

Zhang, N., Kallis, R.P., Ewy, R.G. & Portis, A.R. (2002). Light modulation of Rubisco in Arabidopsis requires a capacity for redox regulation of the larger Rubisco activase isoform. *Proceedings of the National Academy of Sciences* , 99(5), 3330-3334.

Zhou, J., Jiao, F., Wu, Z., Li, Y., Wang, X., He, X., Zhong, W. & Wu, P. (2008). OsPHR2 is involved in phosphate-starvation signaling and excessive phosphate accumulation in shoots of plants. *Plant Physiology* , 146(4), 1673-1686.

Zhu, Y.G., Smith, S.E. & Smith, F.A. (2001). Zinc (Zn)-phosphorus (P) interactions in two cultivars of spring wheat (*Triticum aestivum*L.) differing in P uptake efficiency. *Annals of Botany* , *88* (5), 941-945.

Figure legends

Figure 1

Growth phenotypes of rice plants grown under different inorganic phosphate (Pi) application conditions. (a) shows representative plants grown under different Pi application conditions at the 70th day after germination. White bars indicate a scale of 10 cm. At this stage, plant height (b) and chlorophyll content in leaf blade (c) were examined. (d) shows the dry matter of leaf blade, leaf sheath, and root in rice plants grown under different Pi application conditions. The results are expressed as mean +- SD (n = 6-8). Different alphabets indicate significant differences between different Pi application conditions (Tukey-Kramer's HSD test, $p < 0.05$).

Figure 2

CO_2 assimilation (A) and photosynthetic parameters evaluated by the chlorophyll fluorescence analysis of the change in the internal CO_2 concentration (Ci) in rice leaves. (a) shows the results of A in rice plants grown under 0.06 and 0.6 mM Pi conditions, and (e) shows the results of A in rice plants grown under 0.6 to 3.0 mM Pi conditions. The results of the 0.6 mM Pi treatment are the same in (a) and (e). (b), (c), and (d) show the results of Y(II), Y(NPQ), and Y(NO), respectively, in the rice plants grown under 0.06 and 0.6 mM Pi conditions. (f), (g) and (h) shows the results of Y(II), Y(NPQ), and Y(NO) in rice plants grown under 0.6 to 3.0 mM Pi conditions. The results of 0.6 mM Pi are the same in (b) and (f), (c) and (g), and (d) and (h). (i) shows the initial slope of$A$ toward the increase in Ci under low Ci conditions. (j) shows the Fv/Fm in rice leaves grown under different Pi application conditions. These results are expressed as mean +- SD (n = 4-6). Different alphabets in (i) and (j) indicate significant differences among different Pi application conditions (Tukey-Kramer's HSD test, $p < 0.05$).

Figure 3

Effects of Pi application on the sugar-phosphate and adenylate content in rice leaves. (a) shows the scheme of sugar-phosphate metabolism in the chloroplasts and cytosol. The sugar-phosphate content described as red-characters indicate those quantified in this study. (b) shows the sugar-phosphate content in rice leaf blade. White, blue, dark blue, purple, pink, and red bars indicate low (0.06 mM), control (0.6 mM), 1.2 mM, 1.8 mM, 2.4 mM, and 3.0 mM treatment conditions, respectively. (c) and (d) show adenylate content and ATP/ADP ratio in rice leaf blade. These results are expressed as mean +- SD (n = 3-9). Different alphabets indicate significant differences among different Pi application conditions (Tukey-Kramer's HSD test, $p < 0.05$).

Figure 4

Effects of P toxicity on Rubisco content and activation by Rubisco activase (RCA). (a) shows the leaf nitrogen content in rice leaves, and (b) shows the Rubisco content in rice leaves (n = 3-4). Rubisco activation was calculated from the ratio of the initial to maximum Rubisco activity (c), and the carbamylation potential was calculated from the ratio of the total to the maximum Rubisco activity (d) (n = 3-5). The white and dark gray bars indicate the results of the leaves sampled under illumination and at night, respectively, under the control-Pi conditions. (e) shows the result of the western-blot analysis, which targets RCA in rice leaves. Red arrows and Greek characters indicate the isoforms of RCA. Each sample was loaded on the leaf area

basis (0.02 cm^2). (f) and (g) show the relative content of the total RCA and each isoform evaluated from the western-blot analysis. The RCA content in the control-Pi plants, set as "1" and the relative content is shown. The black, red, and gray characters above the bars indicate the statistical results of the α, β, β^* isoforms, respectively. (h) and (i) show the isoform ratio between α /β and β */β (n = 4). These results are expressed as mean ± SD. Different alphabets indicate the significant difference among different Pi application conditions (Tukey-Kramer's HSD test, $p < 0.05$).

Figure 5

Ascorbate peroxidase (APX) and superoxide dismutase (SOD) activities in rice leaves grown under different Pi application conditions. (a) shows the results of the total, cytosolic, and chloroplastic APX activities evaluated on the leaf area basis. The red, yellow, and green characters above the bars indicate the statistical results of the total, cytosolic, and chloroplastic APX activities, respectively. (b) shows the results of the chloroplastic APX activities evaluated on the chlorophyll basis. (c) shows the results of the total, Fe-, Mn-, and Cu/Zn-SOD activities evaluated on the leaf area basis. The gray and blue characters above the bars indicate the statistical results of the total and the Cu/Zn-SOD activities. These results are expressed as mean ± SD (n = 3). Different alphabets indicate significant differences among different Pi application conditions (Tukey-Kramer's HSD test, $p < 0.05$).

Figure 6

mRNA expression of all Cu/Zn-SOD genes in rice plants. The mRNA expression is expressed on fresh weight (F.W.) (red bars) and 18S ribosome expression (blue bars) basis. These results are expressed as mean ± SD (n = 3-4). Different alphabets indicate significant differences among different Pi application conditions (Tukey-Kramer's HSD test, $p < 0.05$).

Figure 7

Leaf mineral content and metal responsive gene expression in rice leaves grown under different Pi application conditions. The content of each mineral nutrient was quantified on the leaf dry matter basis (a). These results are expressed as mean ± SD (n = 3-4). (b) shows the mRNA expression of the metal-deficiency-responsive genes *ZIP4* ,*IRO2* , and *COPT1* in the leaves. The mRNA expression is expressed on the F.W. (red bars) and 18S ribosome expression (blue bars) basis. These results are expressed as mean ± SD (n = 3-7). Different alphabets indicate significant differences among different Pi application conditions (Tukey-Kramer's HSD test, $p < 0.05$).

Figure 8

mRNA expression involved in phytic acid synthesis and phytic acid content in leaves. (a) shows the scheme of phytic acid synthesis in plants (Penera et al., 2019). (b) shows the mRNA expression of phytic acid synthesis mRNA expression was expressed on the F.W. (red bars) and 18S ribosome expression (blue bars) basis. (c) and (d) show leaf phytic acid content expresses on the F.W. and leaf area basis, respectively. (e) shows the molecular ratio of phytic acid to free Pi in leaves. These results are expressed as mean ± SD (n = 3-4). Different alphabets indicate significant differences among different Pi application conditions (Tukey-Kramer's HSD test, $p < 0.05$).

Figure 9

Scheme of P toxicity in plant cells. Under normal P concentration (a), phytic acid synthesis is maintained to produce its proper concentration in the cytosol, preventing any negative effects of phytic acid on physiological functions within a plant cell. Under excessive Pi accumulation (b), an increase in the cytosolic sugar-phosphate content activates phytic acid synthesis, and an increase in the phytic acid concentration causes Zn insolubilization, which, in turn, decreases Cu/Zn-SOD activities. Simultaneously, RCA content decreases depending on the excessive accumulation of Pi, and photosynthesis is limited by a decrease in electron sink activities, partly because of the decrease in Rubisco activation. The decrease in electron sink activities leads to a decrease in ATP and NADPH consumptions. Subsequently, electrons are accumulated in

PET chain, stimulating reactive oxygen species (ROS) production. ROS accumulation is further intensified by a decrease in Cu/Zn-SOD activity. As a result, higher ROS accumulation triggers leaf necrosis in land plants.

Table 1

The results were expressed as mean ±SD (n = 3-4). The different alphabets indicate the significant differences between each P application conditions (Tukey-Kramer's HSD test, $p < 0.05$).

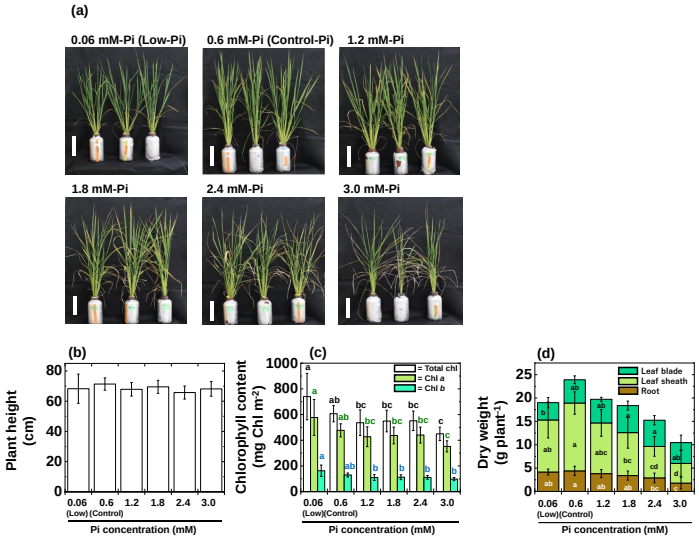

Figure 1

Growth phenotypes of rice plants grown under different inorganic phosphate (Pi) application conditions. (a) shows representative plants grown under different Pi application conditions at the 70th day after germination. White bars indicate a scale of 10 cm. At this stage, plant height (b) and chlorophyll content in leaf blade (c) were examined. (d) shows the dry matter of leaf blade, leaf sheath, and root in rice plants grown under different Pi application conditions. The results are expressed as mean ± SD (n = 6-8). Different alphabets indicate significant differences between different Pi application conditions (Tukey-Kramer's HSD test, $p < 0.05$).

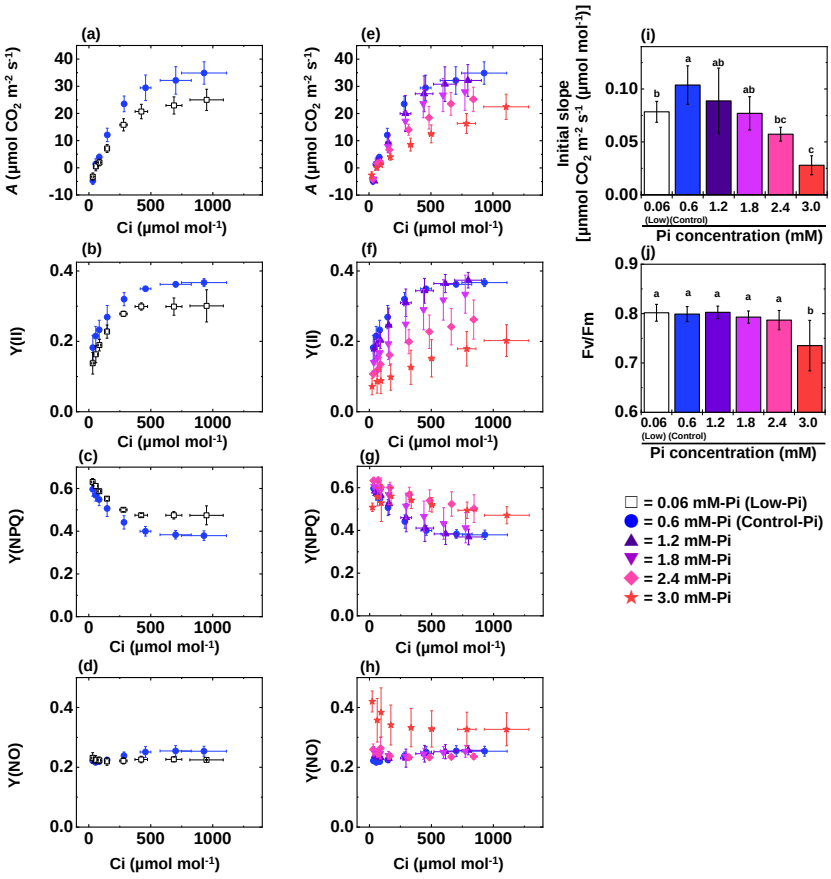

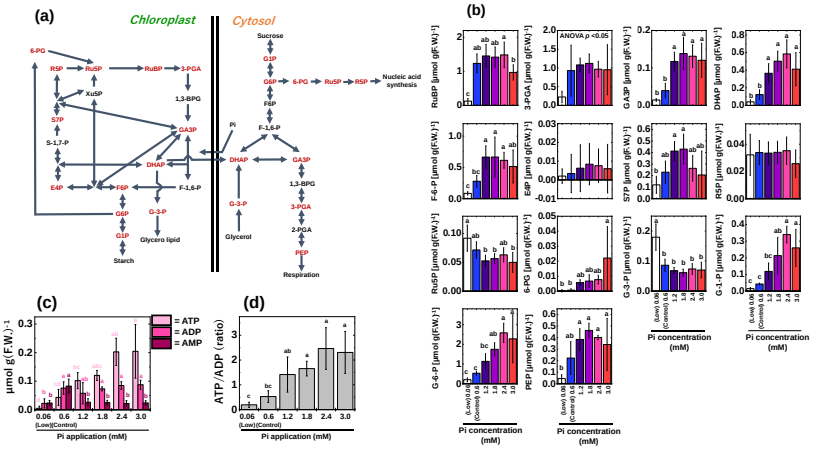

Figure 3

Effects of Pi application on the sugar-phosphate and adenylate content in rice leaves. (a) shows the scheme of sugar-phosphate metabolism in the chloroplasts and cytosol. The sugar-phosphate content described as red-characters indicate those quantified in this study. (b) shows the sugar-phosphate content in rice leaf blade. White, blue, dark blue, purple, pink, and red bars indicate low (0.06 mM), control (0.6 mM), 1.2 mM, 1.8 mM, 2.4 mM, and 3.0 mM treatment conditions, respectively. (c) and (d) show adenylate content and ATP/ADP ratio in rice leaf blade. These results are expressed as mean ± SD (n = 3-9). Different alphabets indicate significant differences among different Pi application conditions (Tukey-Kramer's HSD test, $p < 0.05$).

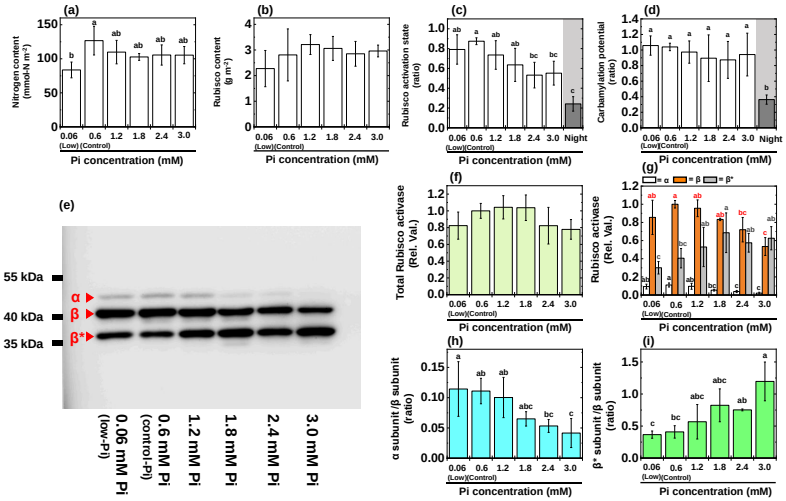

Figure 4

Effects of P toxicity on Rubisco content and activation by Rubisco activase (RCA). (a) shows the leaf nitrogen content in rice leaves, and (b) shows the Rubisco content in rice leaves (n = 3-4). Rubisco activation was calculated from the ratio of the initial to maximum Rubisco activity (c), and the carbamylation potential was calculated from the ratio of the total to the maximum Rubisco activity (d) (n = 3-5). The white and dark gray bars indicate the results of the leaves sampled under illumination and at night, respectively, under the control-Pi conditions. (e) shows the result of the western-blot analysis, which targets RCA in rice leaves. Red arrows and Greek characters indicate the isoforms of RCA. Each sample was loaded on the leaf area basis (0.02 cm^2). (f) and (g) show the relative content of the total RCA and each isoform evaluated from the western-blot analysis. The RCA content in the control-Pi plants, set as "1" and the relative content is shown. The black, red, and gray characters above the bars indicate the statistical results of the *α, β, β** isoforms, respectively. (h) and (i) show the isoform ratio between *α*/*β* and *β**/*β* (n = 4). These results are expressed as mean ± SD. Different alphabets indicate the significant difference among different Pi application conditions (Tukey-Kramer's HSD test, $p < 0.05$).

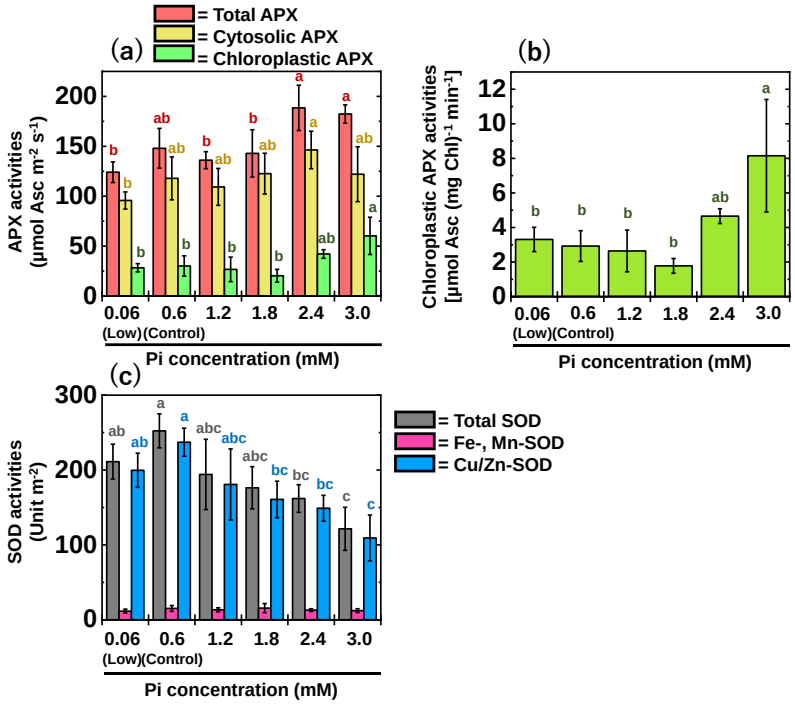

Figure 5

Ascorbate peroxidase (APX) and superoxide dismutase (SOD) activities in rice leaves grown under different Pi application conditions. (a) shows the results of the total, cytosolic, and chloroplastic APX activities evaluated on the leaf area basis. The red, yellow, and green characters above the bars indicate the statistical results of the total, cytosolic, and chloroplastic APX activities, respectively. (b) shows the results of the chloroplastic APX activities evaluated on the chlorophyll basis. (c) shows the results of the total, Fe-, Mn-, and Cu/Zn-SOD activities evaluated on the leaf area basis. The gray and blue characters above the bars indicate the statistical results of the total and the Cu/Zn-SOD activities. These results are expressed as mean ± SD (n = 3). Different alphabets indicate significant differences among different Pi application conditions (Tukey-Kramer's HSD test, $p < 0.05$).

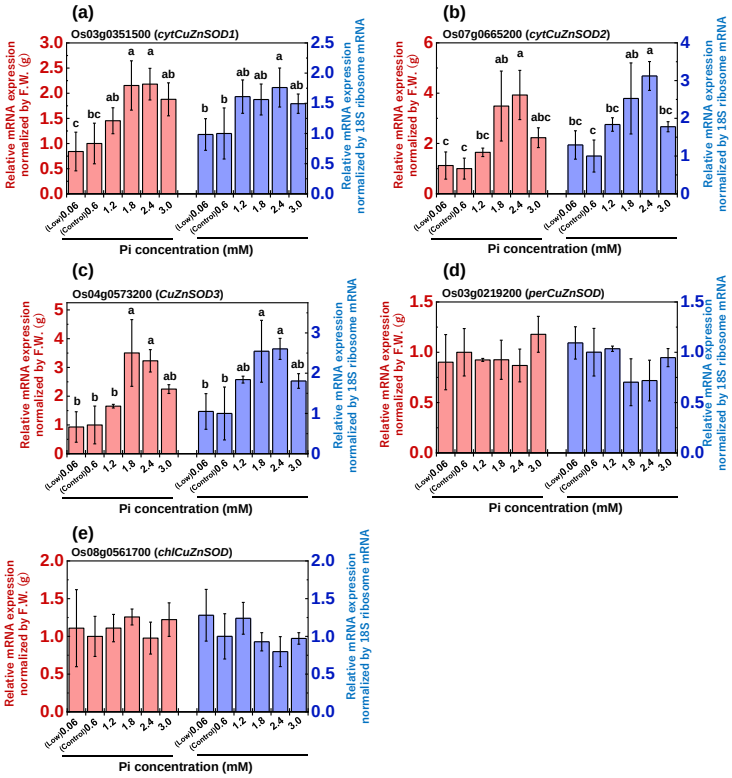

Figure 6

mRNA expression of all Cu/Zn-SOD genes in rice plants. The mRNA expression is expressed on fresh weight (F.W.) (red bars) and 18S ribosome expression (blue bars) basis. These results are expressed as mean ± SD (n = 3-4). Different alphabets indicate significant differences among different Pi application conditions (Tukey-Kramer's HSD test, $p < 0.05$).

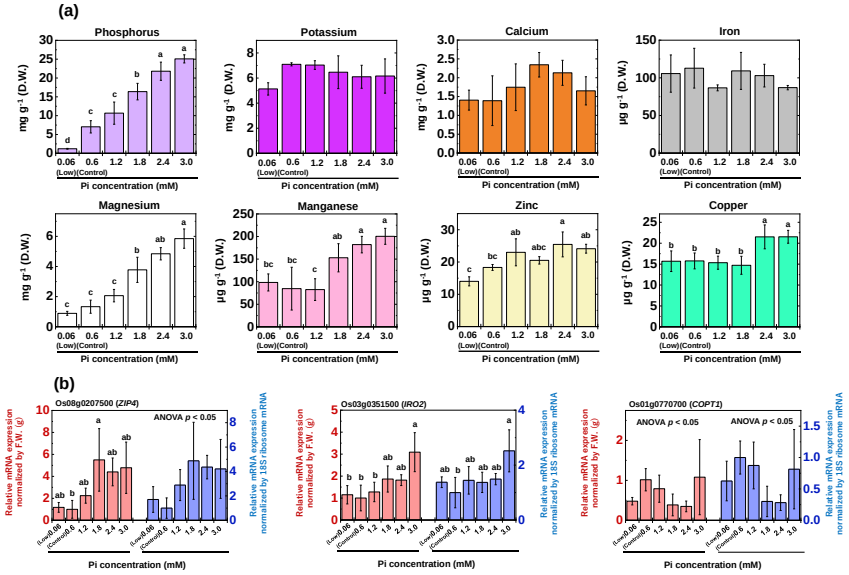

Figure 7

Leaf mineral content and metal responsive gene expression in rice leaves grown under different Pi application conditions. The content of each mineral nutrient was quantified on the leaf dry matter basis (a). These results are expressed as mean ± SD (n = 3-4). (b) shows the mRNA expression of the metal-deficiency-responsive genes *ZIP4*, *IRO2*, and *COPT1* in the leaves. The mRNA expression is expressed on the F.W. (red bars) and 18S ribosome expression (blue bars) basis. These results are expressed as mean ± SD (n = 3-7). Different alphabets indicate significant differences among different Pi application conditions (Tukey-Kramer's HSD test, $p < 0.05$).

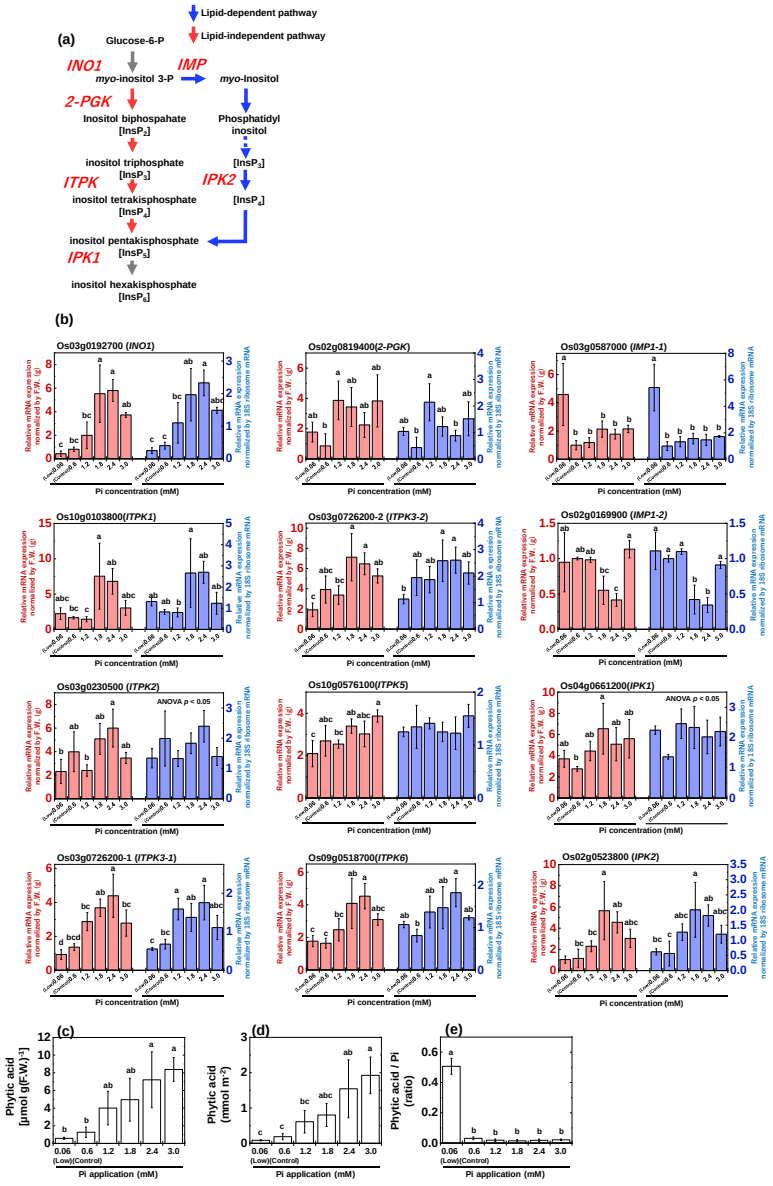

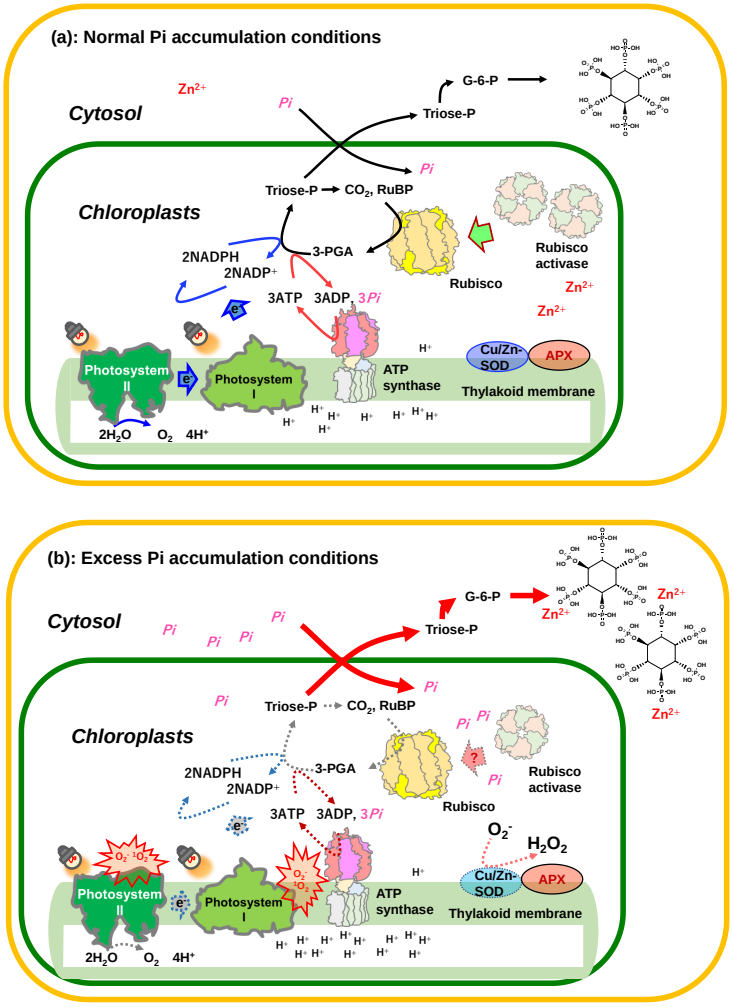

Tables

Table 1
Pi and Po content in rice leaf blade

	Pi concentration					
	0.06 mM	0.6 mM	1.2 mM	1.8 mM	2.4 mM	3.0 mM
Pi (mmol m^{-2})	0.450 ± 0.018^{d}	9.16 ± 1.86^{cd}	26.0 ± 5.71^{c}	38.8 ± 1.89^{bc}	61.5 ± 13.0^{b}	79.2 ± 14.0^{a}
Pi (μmol g^{-1}[FW])	2.90 ± 0.48^{d}	57.0 ± 20.2^{cd}	114.3 ± 16.2^{c}	193.1 ± 18.7^{bc}	295.4 ± 66.8^{b}	365.4 ± 32.4^{a}
Po (mmol m^{-2})	0.180 ± 0.036^{c}	2.33 ± 1.19^{bc}	10.0 ± 2.95^{b}	7.40 ± 5.76^{bc}	14.87 ± 5.45^{a}	17.2 ± 3.9^{a}
Po (μmol g^{-1}[FW])	1.21 ± 0.40^{c}	14.9 ± 9.12^{bc}	44.1 ± 12.1^{b}	36.3 ± 27.1^{bc}	58.8 ± 20.5^{a}	75.0 ± 20.0^{a}

(n = 3-4 mean ± SD)

The results were expressed as mean ± SD (n = 3-4). The different alphabets indicate the significant differences between each P application conditions (Tukey-Kramer's HSD test, $p < 0.05$).